AGU PUBLICATIONS

Geochemistry, Geophysics, Geosystems

RESEARCH ARTICLE
10.1002/2015GC005800

Magmatic water contents determined through clinopyroxene: Examples from the Western Canary Islands, Spain

Franz A. Weis[1,2], Henrik Skogby[1], Valentin R. Troll[2,3], Frances M. Deegan[2,4], and Börje Dahren[2]

[1]Department of Geosciences, Swedish Museum of Natural History, Stockholm, Sweden, [2]Department of Earth Sciences, Center of Experimental Mineralogy, Petrology and Geochemistry, Uppsala University, Uppsala, Sweden, [3]Department of Physics (GEOVOL), University of Las Palmas de Gran Canaria, Las Palmas de Gran Canaria, Spain, [4]Department of Geological Science, Stockholm University, Stockholm, Sweden

Key Points:
- Hydrogen-associated structural defects are experimentally rehydrated in degassed pyroxene
- Rehydrated NAMs yield parental magmatic H_2O contents
- Rehydrating NAMs can become a method for reconstructing magmatic H_2O contents

Correspondence to:
F. A. Weis,
franz.weis@nrm.se

Citation:
Weis, F. A., H. Skogby, V. R. Troll, F. M. Deegan, and B. Dahren (2015), Magmatic water contents determined through clinopyroxene: Examples from the Western Canary Islands, Spain, *Geochem. Geophys. Geosyst.*, *16*, 2127–2146, doi:10.1002/2015GC005800.

Received 2 MAR 2015
Accepted 1 JUN 2015
Accepted article online 3 JUN 2015
Published online 14 JUL 2015

Abstract Water is a key parameter in magma genesis, magma evolution, and resulting eruption styles, because it controls the density, the viscosity, as well as the melting and crystallization behavior of a melt. The parental water content of a magma is usually measured through melt inclusions in minerals such as olivine, a method which may be hampered, however, by the lack of melt inclusions suitable for analysis, or postentrapment changes in their water content. An alternative way to reconstruct the water content of a magma is to use nominally anhydrous minerals (NAMs), such as pyroxene, which take up low concentrations of hydrogen as a function of the magma's water content. During magma degassing and eruption, however, NAMs may dehydrate. We therefore tested a method to reconstruct the water contents of dehydrated clinopyroxene phenocrysts from the Western Canary islands (n = 28) through rehydration experiments followed by infrared and Mössbauer spectroscopy. Employing currently available crystal/melt partitioning data, the results of the experiments were used to calculate parental water contents of 0.71 ± 0.07 to 1.49 ± 0.15 wt % H_2O for Western Canary magmas during clinopyroxene crystallization at upper mantle conditions. This H_2O range is in agreement with calculated water contents using plagioclase-liquid-hygrometry, and with previously published data for mafic lavas from the Canary Islands and comparable ocean island systems elsewhere. Utilizing NAMs in combination with hydrogen treatment can therefore serve as a proxy for pre-eruptive H_2O contents, which we anticipate becoming a useful method applicable to mafic rocks where pyroxene is the main phenocryst phase.

1. Introduction

The concentration of water in magma plays a significant role in its genesis, its differentiation, and its eventual eruption, since water influences the melting and solidification behavior as well as the density and viscosity of magmatic liquids [e.g., *Woods and Koyaguchi*, 1993; *Roggensack et al.*, 1997; *Cashman*, 2004; *Malfait et al.*, 2014; *Sides et al.*, 2014]. Water-rich magmas generally tend to erupt in a more explosive fashion [e.g., *Woods and Koyaguchi*, 1993; *Dingwell*, 1996; *Cashman*, 2004] and in order to advance our understanding of past and future eruption behavior and changes in eruptive styles, it is important to quantify magmatic water contents in the natural range of magmas that erupted throughout Earth's history up to the present day. Various methods exist to determine preeruptive magmatic water contents, such as the analysis of phase assemblages and melt compositions [e.g., *Rutherford et al.*, 1985; *Rutherford and Devine*, 1996; *Hammer and Rutherford*, 2003; *Longpré et al.*, 2009], feldspar-liquid hygrometry [*Lange et al.*, 2009; *Waters and Lange*, 2015], or the measurement of volatile contents directly from quenched volcanic glass or melt inclusions [e.g., *Dixon et al.*, 1997; *Dixon and Clague*, 2001; *Wallace*, 2005; *Walker et al.*, 2003; *Vigouroux et al.*, 2012]. Melt inclusions in particular have become a common and useful tool for constraining the volatile content of magma [e.g., *Belkin et al.*, 1998; *Thomas*, 2000; *Wallace*, 2005; *Moune et al.*, 2007; *Hauri et al.*, 2011; *Plank et al.*, 2013]. However, this approach cannot be universally employed because isolated melt inclusions may not always be present in the size suitable for analysis, they may be completely absent in a sample, or they may have undergone varying degrees of postentrapment water loss or gain [e.g., *Massare et al.*, 2002; *Portnyagin et al.*, 2008; *Baker*, 2008; *Esposito et al.*, 2014; *Gaetani et al.*, 2014; *Le Voyer et al.*, 2014].

An alternative method to determine the water content of a magma is to use nominally anhydrous minerals (NAMs) [e.g., *Abaud et al.*, 2004; *Wade et al.*, 2008; *Nazzareni et al.*, 2011; *Hamada et al.*, 2011; *Okumura*, 2011]. Nominally anhydrous minerals, such as clinopyroxene (cpx), incorporate hydrogen in association with

structural defects (e.g., charge deficiencies) during growth from a hydrous magma. However, the stability of this hydrogen under eruptive processes cannot be taken for granted. Hydrogen diffusion kinetics in pyroxenes, in particular, have been well studied regarding hydration, dehydration, self-diffusion, and dependence on iron content [*Hercule and Ingrin*, 1999; *Ingrin and Skogby*, 2000; *Woods et al*., 2000; *Ingrin and Blanchard*, 2006; *Sundvall et al*., 2009; *Sundvall and Skogby*, 2011]. Results from these studies demonstrate that hydrogen diffusion and subsequent equilibration for clinopyroxenes with $X_{Fe/(Fe+Mg)} > 0.07$ occurs within minutes to hours, with kinetics similar to those of hydrogen self-diffusion (H-D exchange) [see review by *Ingrin and Blanchard*, 2006]. Hydrogen diffusion in or out of pyroxene crystals follows the reversible redox reaction:

$$OH^- + Fe^{2+} \leftrightarrow O^{2-} + Fe^{3+} + 1/2\ H_2 \quad \text{(R1)}$$

where the exchange of hydrogen ions (protons) is counterbalanced by a flux of electron holes [e.g., *Skogby and Rossman*, 1989; *Skogby*, 1994; *Bromiley et al*., 2004; *Koch-Müller et al*., 2007; *Sundvall and Skogby*, 2011]. Depending on eruption style and fluid pressure, clinopyroxenes may rapidly lose parts of their hydrous content according to redox-reaction (R1). Upon magma degassing, for example, NAMs are expected to dehydrate due to equilibration to decreasing fluid pressures [e.g., *Hamada et al*., 2011]. Further, while crystals in fast erupted and quenched pyroclastic materials may not, clinopyroxenes in slower cooling lavas may undergo extensive dehydration [e.g., *Woods et al*., 2000; *Wade et al*., 2008]. The hydrogen-associated defects in the crystal structure, however, will remain after dehydration and cooling, because they are governed by cation and vacancy diffusion with kinetics many orders of magnitude slower than reaction (R1) [e.g., *Ingrin and Skogby*, 2000; *Ingrin and Blanchard*, 2006; *Cherniak and Dimanov*, 2010]. Clinopyroxene is therefore expected to "keep a memory" of its initial hydrogen content during original crystallization, a feature that can be exploited as a proxy for parental magmatic water contents. Here we focus on natural samples of partly dehydrated clinopyroxene from mafic alkaline lavas (basanites and ankaramite) and an ankaramite dyke intrusion from the Central and Western Canary archipelago (Tenerife, La Palma, and El Hierro). In these samples, clinopyroxene is the key mineral phase for our investigation, as feldspar phenocrysts are not always present, while olivine is often already in a state of resorption [e.g., *Longpré et al*., 2009; *Manconi et al*., 2009]. We reconstructed the original water contents of the clinopyroxene crystals (n = 28) by performing a series of rehydration experiments and subsequently measuring their rehydrated water contents using Fourier transformed infrared spectroscopy (FTIR). By applying calculated partition coefficients for clinopyroxene and basaltic melt [e.g., *Hauri et al*., 2006; *Wade et al*., 2008; *O'Leary et al*., 2010], the preeruptive water contents of the host magmas were determined. In order to test the validity of our results, we compared our calculated magmatic water contents to values determined through feldspar hygrometry and through an in-depth comparison with the wider range of previously published H_2O data for the Canary Islands and similar ocean island systems elsewhere.

2. Geological Setting

The Canary archipelago is a 600 km long chain of seven major volcanic islands off NW Africa (Figure 1a). The islands are built upon oceanic crust with an age of ~180 Ma at the east and of ~155 Ma toward the west of the island chain [e.g., *Bosshard and Macfarlane*, 1970; *Hoernle*, 1998; *Hansteen and Troll*, 2003]. The ages of the oldest erupted rocks on each island show a systematic younging toward the west of the archipelago. For instance, the oldest volcanic rocks on Lanzarote are ~20 Ma, while those on La Palma and El Hierro are only ≤4 and ≤1.3 Ma, respectively [*McDougall and Schmincke*, 1976; *LeBas et al*., 1986; *Carracedo et al*., 1998; *Klügel*, 1998; *Guillou et al*., 2004; *Longpré et al*., 2008]. The origin of the Canary archipelago was initially linked to lithospheric fracturing in connection to the Atlas mountains [e.g., *Anguita and Hernán*, 1975, 2000], but the mantle plume model is currently more widely accepted as the cause for Canary Island magmatism. The plume model is based on the progressive chronological, geomorphological, and geochemical history of the island chain and on a seismic mantle anomaly that has been imaged to the core-mantle boundary [see *Hoernle and Schmincke*, 1993a; *Hoernle et al*., 1995; *Carracedo et al*., 1998; *Montelli et al*., 2004, 2006; *Geldmacher et al*., 2005; *Deegan et al*., 2012; *Zaczek et al*., 2015].

3. Samples

Most rock samples used in this study are basanite lavas from the island of La Palma (n = 8) (Figures 1b and 1c). One further ankaramite lava sample is from El Hierro, the youngest and westernmost island in the Canary archipelago (Figures 1a and 1b), and another ankaramite sample is from a dyke intrusion on

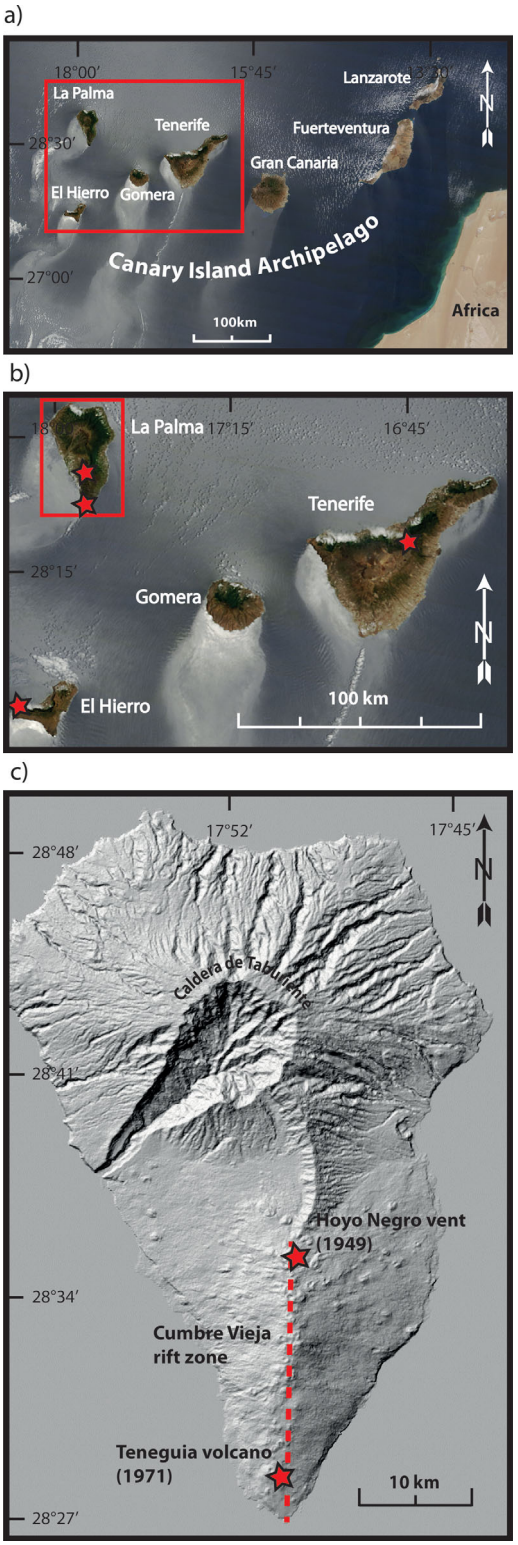

Figure 1. (a–c) Map showing the location of La Palma, El Hierro, and Tenerife in the Western Canary archipelago (sources: NASA, GRAFCAN). Red stars mark the sampling locations. Lava samples from La Palma were taken from the Hoyo Negro vent (1949 eruption) and the Teneguia volcano (1971 eruption) on the Cumbre Vieja rift (marked by red broken line). Complementary samples were taken from the Lomo Negro ankaramite lava flow on Western El Hierro and from an ankaramite dyke in the Northeast rift zone (NERZ) on Tenerife.

Tenerife (see also below; Figure 1b). La Palma and El Hierro are currently in their shield stages of ocean island evolution [*Carracedo et al*., 2001; *Klügel et al*., 2005], while Tenerife has concluded its shield stage of growth and now exhibits more differentiated volcanic activity [*Guillou et al*., 2004; *Carracedo and Troll*, 2013]. A full description of the geology of La Palma is presented in *Carracedo et al*. [2001, and references therein], but a short summary is also provided below. A summary for El Hierro and Tenerife can be found in *Ancochea et al*. [1990], *Carracedo et al*. [2001], and *Carracedo and Troll* [2013].

3.1. La Palma

La Palma can be divided into three main geological units:

1. A basal complex (3–4 Ma) that comprises prevolcanic sedimentary rocks and a Pliocene seamount sequence with an exposed plutonic core. The seamount-related rocks were uplifted and tilted, and are exposed today inside the deeply eroded Caldera de Taburiente in the northern part of the island [*Staudigel and Schmincke*, 1984].
2. A series of volcanic edifices (the Taburiente and Garafia volcanoes; 1.8 Ma to 410 ka) are superimposed on these seamount and plutonic lithologies and make up most of the northern part of the present island.
3. The Cumbre Vieja ridge (~125 ka to present) is a prominent north-south trending ridge (Figure 1c), which developed after the Taburiente system shut down [e.g., *Carracedo et al*., 2001; *Walter and Troll*, 2003]. The Cumbre Vieja ridge is the currently active volcanic system on La Palma and makes up the southern half of the island. Prehistoric and historic eruptions of the Cumbre Vieja were frequent, with historic events recorded in 1470, 1585, 1646, 1677, 1712, 1949, and 1971 [e.g., *Abdel-Monem et al*., 1972; *Klügel et al*., 2000; *Carracedo et al*., 2001].

Lava compositions of the Cumbre Vieja are dominantly mafic alkali basalts and basanites, but small volume phonolite domes also occur [*Klügel et al*., 2000, 2005]. Most historic lavas on the Cumbre Vieja rift are chemically and mineralogically zoned and often carry a range of xenoliths, including ultramafic cumulates, MORB-type basalts, and alkaline gabbros, plus a range of felsic fragments [*Araña and Ibarrola*, 1973; *Carracedo et al*., 2001; *Klügel et al*., 2005]. Samples investigated in this study are basanite lavas (Figure 2) from the 1949 eruption (Hoyo Negro vent) and from the 1971

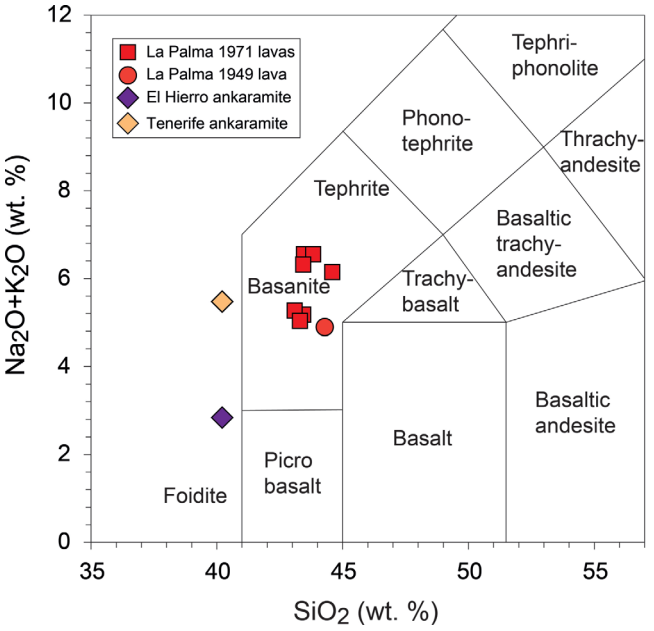

Figure 2. Total alkalis versus silica (TAS) diagram, showing the composition of the rock samples used in this study. The majority of the samples plot in the basanite field, which is the most common lava type in the Western Canary Islands. Boundaries for the individual fields were drawn after *Irvine and Baragar* [1971] and the nomenclature is adopted from *Le Maitre et al*. [1989].

Teneguia eruption. The samples of the two eruptions are treated as individual batches of magma, each having undergone differentiation processes. The lavas contain clinopyroxene, kaersutite, olivine, and occasionally feldspar phenocrysts of up to 3 mm in size on average. These larger crystals are embedded in a fine-grained groundmass of plagioclase, clinopyroxene, and olivine. Some samples include small gabbro or felsic xenoliths (Table 1), but these were not investigated in this study. All lava samples contain vesicles, reflecting syneruptive magma degassing.

3.2. Tenerife and El Hierro

To complement the La Palma sample suite and to allow a regional comparison of our data, we also investigated an ankaramite dyke sample from the ~0.8–0.5 Ma Northeast rift zone (NERZ) on Tenerife [*Carracedo et al*., 2011; *Deegan et al*., 2012], and a sample from the prehistoric Lomo Negro ankaramite lavas from the Western edge of El Hierro (Figures 1a, 1b, and 2) [*Carracedo et al*., 2001]. These two samples were chosen for their high content of large (>3 mm) clinopyroxene phenocrysts. For a detailed geological background on the samples from Tenerife and El Hierro, the reader is referred to *Carracedo et al*. [2001], *Delcamp et al*. [2010, 2012], *Deegan et al*. [2012], and *Manconi et al*. [2009].

4. Methods

Rock samples (n = 10) were crushed to obtain loose clinopyroxene crystals of a size suitable for analysis (≥300 μm). These were hand-picked under a binocular microscope and individual clinopyroxene crystals were then mounted in thermoplastic resin for further processing. With the help of crystal morphology and optical microscopy (extinction angles), the selected crystals (n = 28) were oriented along their crystallographic *c* axis and their (100) and (010) crystal faces, on which the directions of the main refractive indices (α, β, and γ) occur. Various particle size-grades of Al_2O_3-grinding paper were used to polish the oriented crystals to a thickness of a few hundred micrometers.

An aliquot of each rock sample was subsequently powdered for major element analysis using an automated Retsch RM200 agate mortar at the Department of Earth Sciences, Uppsala University.

Table 1. Sample Set Used in This Study

Sample	Eruption	Sample Description	No. of cpx Analyzed
La Palma			
LP1971/E	Teneguía, 1971	Slightly vesicular basanite with olivine and pyroxene phenocrysts, kaersutite, and plagioclase	3
LP1971/F	Teneguía, 1971	Slightly vesicular basanite with olivine and pyroxene phenocrysts, kaersutite, and plagioclase	3
LP1971/H	Teneguía, 1971	Basanite with olivine and pyroxene phenocrysts, kaersutite, and plagioclase	3
LP1971/1	Teneguía, 1971	Vesicular basanite, some pyroxene phenocrysts, includes small quartz/feldspar xenoliths	3
LP1971/2	Teneguía, 1971	Vesicular basanite with pyroxene and olivine phenocrysts, includes gabbro xenolith	2
LP1971/3	Teneguía, 1971	Vesicular basanite with pyroxene and large olivine phenocrysts	3
LP1971/209	Teneguía, 1971	Vesicular, dark gray basanite with olivine and pyroxene phenocrysts	3
LP1949-1	Hoyo Negro vent, 1949	Basanite with olivine and pyroxene phenocrysts	3
Tenerife			
NER57[a]	Northeast rift zone, prehistoric	Ankaramite dyke with abundant pyroxene and olivine phenocrysts	2
El Hierro			
EH-Ank	Lomo Negro, prehistoric	Ankaramite, pahoehoe lava flow dark, slightly vesicular, pyroxene and olivine phenocrysts	3

[a]Sample previously described in *Deegan et al.* [2012].

4.1. Whole-Rock Geochemical Analysis

Whole-rock powders (n = 10) were analyzed for major elements at Acme Analytical Labs Ltd in Vancouver, Canada. Major elements were measured by Inductively Coupled Plasma Optical Emission Spectrometry (ICP-OES) on a Spectro Arcos system. Sample preparation included mixing of powdered rock material with a $LiBO_2/Li_2B_4O_7$ flux agent before sample fusion in a furnace. Prior to measurement, the sample bead was dissolved by applying dilute nitric acid digestion. Data quality during analysis was monitored using two certified, internal reference materials. Accuracy of the standard measurements is $<0.2\%$ for SiO_2, Al_2O_3, Fe_2O_3, MgO, CaO, Na_2O, K_2O, TiO_2, P_2O_5, MnO, and Cr_2O_3. Duplicate analyses have a reproducibility of $<5\%$ (2 s. d.) for all oxides. The iron content is reported as Fe_2O_3 (Table A1).

4.2. Electron Probe Microanalysis

Electron probe microanalyses (EPMA) of major elements (Al, Ti, Fe, Mg, Na, K, Si, Ca, Mn, and Cr) in clinopyroxene and feldspar crystals were carried out at the Department of Earth Sciences, Uppsala University using a Field Emission-EPMA JXA-8530F JEOL superprobe. Between five and eight spots were analyzed on each crystal using a beam current of 10 nA with an acceleration voltage of 15 kV. The beam diameter was set to 1 μm. Standards used were fayalite (Fe_2SiO_4) for Fe, magnesium oxide (MgO) for Mg, pyrophanite ($MnTiO_3$) for Mn and Ti, aluminum oxide (Al_2O_3) for Al, wollastonite ($CaSiO_3$) for Ca and Si, chromium oxide (Cr_2O_3) for Cr, nickel oxide (NiO) for Ni as well as albite ($NaAlSi_3O_8$), orthoclase ($KAlSi_3O_8$) and apatite ($Ca_5(PO_4)_3(OH,F,Cl)$) for Na, K, and P, respectively. Several crystals showed weak zonation in backscattered electron (BSE) images and for each crystal an average composition was calculated from all analyzed spots. Estimated uncertainties (2 s.d.) for major elements are $\pm 1\%$. From the obtained weight percentages, the number of atoms per formula unit in each crystal was calculated on the basis of a four cation-normalization. In order to distinguish between and quantify Fe^{2+} and Fe^{3+} in clinopyroxenes, the results from the Mössbauer analysis were applied (see section 4.5).

4.3. Rehydration Experiments

In order to rehydrate the hydrogen-associated defects in dehydrated clinopyroxenes, the crystals were heated under a stream of H_2 gas for either several 16 h long intervals or for a single 24 h or 26 h interval (see Table 2 for details). Rehydration experiments were performed at a temperature of 700°C and an ambient pressure of 1 atm. Under these conditions hydrogen diffusion coupled to redox reaction (R1) has been shown to be active [*Skogby and Rossman*, 1989; *Skogby*, 1994; *Bromiley et al.*, 2004; *Koch-Müller et al.*, 2007; *Sundvall and Skogby*, 2011]. Clinopyroxene crystals in this study show $X_{Fe/(Fe+Mg)} > 0.18$ (Table A3) and thus the kinetics for R1 are similar to the kinetics for hydrogen self-diffusion [*Ingrin and Blanchard*, 2006]. Under the set conditions the reaction kinetics for hydrogen self-diffusion are $\log D = -11.5$ m^2/s and hence almost

Table 2. Water Contents of Canary Clinopyroxenes Before and After Hydrogen Treatment[a]

	Water Content (ppm weight H_2O)						
Sample	Untreated	16 h H_2	24 h H_2	26 h H_2	32 h H_2	48 h H_2	56 h H_2
La Palma							
LP1971-E(1)	102	347	n.d.[b]	n.d.	346	n.d.	387
LP1971-E(2)	83	n.d.	n.d.	336	n.d.	n.d.	n.d.
LP1971-E(3)	74	n.d.	n.d.	345	n.d.	n.d.	n.d.
LP1971-F(1)	78	340	n.d.	n.d.	331	n.d.	369
LP1971-F(2)	87	n.d.	n.d.	312	n.d.	n.d.	n.d.
LP1971-F(3)	94	n.d.	n.d.	386	n.d.	n.d.	n.d.
LP1971-H(1)	38	218	n.d.	n.d.	293	n.d.	272
LP1971-H(2)	89	n.d.	n.d.	351	n.d.	n.d.	n.d.
LP1971-H(3)	74	n.d.	n.d.	313	n.d.	n.d.	n.d.
LP1971-1(1)	164	344	n.d.	n.d.	377	393	n.d.
LP1971-1(2)	115	n.d.	n.d.	416	n.d.	n.d.	n.d.
LP1971-1(3)	130	n.d.	n.d.	385	n.d.	n.d.	n.d.
LP1971-2(1)	168	362	n.d.	n.d.	357	n.d.	n.d.
LP1971-2 2)	164	n.d.	447	n.d.	n.d.	n.d.	n.d.
LP1971-3(1)	21	255	n.d.	n.d.	308	n.d.	n.d.
LP1971-3(2)	40	n.d.	344	n.d.	n.d.	n.d.	n.d.
LP1971-3(3)	48	n.d.	442	n.d.	n.d.	n.d.	n.d.
LP1971-209(1)	65	248	n.d.	n.d.	252	n.d.	n.d.
LP1971-209(2)	b.d.[c]	n.d.	296	n.d.	n.d.	n.d.	n.d.
LP1971-209(3)	b.d	n.d.	269	n.d.	n.d.	n.d.	n.d.
LP1949-1(1)	28	n.d.	361	n.d.	n.d.	n.d.	n.d.
LP1949-1(2)	26	n.d.	359	n.d.	n.d.	n.d.	n.d.
LP1949-1(3)	18	n.d.	340	n.d.	n.d.	n.d.	n.d.
Tenerife							
NER57(1)	107	235	n.d.	n.d.	n.d.	n.d.	n.d.
NER57(2)	44	n.d.	n.d.	202	n.d.	n.d.	n.d.
El Hierro							
EH-Ank(1)	92	226	n.d.	n.d.	239	258	n.d.
EH-Ank(2)	63	n.d.	n.d.	245	n.d.	n.d.	n.d.
EH-Ank(3)	52	n.d.	n.d.	243	n.d.	n.d.	n.d.

[a]Estimated uncertainty for water contents is ±10%.
[b]n.d.: not determined.
[c]b.d.: below detection.

4.5 orders of magnitude higher than for vacancy diffusion ($\log D \leq -16$ m^2/s) [*Ingrin and Skogby*, 2000; *Ingrin and Blanchard*, 2006; *Cherniak and Dimanov*, 2010]. For the given temperature and time intervals, resetting of structural defects is therefore not expected.

The crystals were kept in a gold sample holder and placed into the middle of a horizontal glass-tube furnace after the target temperature had been reached. The temperature was controlled with a Pt_{100}–$Pt_{90}Rh_{10}$ thermocouple placed directly above the samples, which has an estimated uncertainty of ±2°C. Prior to the heating process, the glass tube was filled with CO_2 so that reaction between the minerals and ambient oxygen as well as an explosion of the hydrogen gas was prevented. Clinopyroxenes were then heated. After thermal annealing, the glass tube was again filled with CO_2 and the crystals were removed from the furnace. Heating and cooling times of the samples for this method are on the order of ∼1 min.

4.4. FTIR Spectroscopy

Before and after hydrogen treatment, polarized FTIR spectra in the range 2000–5000 cm^{-1} were acquired on the oriented clinopyroxene crystals along the directions of the main refractive indices (α, β, and γ) in order to obtain the total absorbance: $A_\alpha + A_\beta + A_\gamma = A_{total}$. The polished crystals were analyzed with a Bruker Equinox 55 spectrometer equipped with a NIR source (halogen lamp), a CaF_2 beamsplitter, a wiregrid polarizer (KRS-5), and an InSb detector. Crystal thickness varied between 150 and 800 μm, with most crystals having a thickness between 200 and 400 μm for both the (100) and (010) orientations. Cracks and inclusions in the crystals were avoided by applying small apertures (100–400 μm) for masking during analysis. In some cases impurities were present in the beam path, but these appeared not to have had any significant effect on the OH range of the spectra. For each individual spectrum, 128 scans were performed and averaged. The obtained spectra were baseline corrected by a polynomial function and the OH bands were fitted with the

software PeakFit. The corresponding water contents were then calculated using both the wavenumber-dependent calibration function established by *Libowitzky and Rossman* [1997] and the mineral-specific (augite) calibration of *Bell et al*. [1995].

4.5. Mössbauer Spectroscopy

The oxidation states of iron in clinopyroxenes before and, where possible, after treatment with hydrogen were obtained by Mössbauer spectroscopy. Powdered crystal separates were analyzed with a ^{57}Co standard source (active diameter 5.0 mm), while selected single crystals were powdered and analyzed with a point source (active diameter 0.5 mm). Several powdered crystals (10 mg in total) from individual rock samples were mixed and ground with a transoptic resin and pressed to a thin disc under mild heat (150°C) for analysis with the standard source. The powdered single crystals were mixed and ground with thermoplastic resin and formed into a ~1 mm^3 cylinder that was mounted on a strip of tape for analysis with the point source. The Mössbauer measurements were performed at incident angles of 90° and 54.7° to the γ rays for the point and the standard source, respectively. All obtained spectra were calibrated against an α-Fe foil, folded, and reduced from 1024 to 512 channels. The spectra fitting was carried out with both the Mössbauer spectral analysis software RECOIL [cf., *Rancourt and Ping*, 1991] and MossA [cf., *Prescher et al*., 2012]. During the fitting process, one doublet each was assigned to Fe^{2+} and Fe^{3+} in the M1 and M2 octahedral positions. From the area of the doublets, the percentage of each oxidation state relative to the total iron content of the sample was obtained, assuming similar recoil-free fractions for Fe^{2+} and Fe^{3+}. The estimated analytical error for the obtained Fe^{m+}/Fe_{total} ratios is ±1%. No crystal specific compositional analysis or determination of hydrogen content before and after annealing was carried out on the Mössbauer sample set due to limitation in crystal size and the destructive nature of sample preparation.

4.6. Magmatic Water Content Calculation

Parental magmatic water contents of an equilibrium magma from which the studied clinopyroxene crystals formed were then calculated using the obtained clinopyroxene water contents after rehydration and utilizing appropriate partition coefficients for H_2O. To calculate partition coefficients for water between clinopyroxene and basaltic melt, we employed the chemical data from the EPMA and the equation of *O'Leary et al*. [2010] ($\ln D = -4.2(\pm 0.2) + 6.5(\pm 0.5)^{VI}[Al^{3+}]\text{-}1.0(\pm 0.2)[Ca^{2+}]$). This equation is specifically designed for Ca-rich clinopyroxene, and is based on the amount of tetrahedral aluminum that is strongly interlinked with hydrogen incorporation into clinopyroxene due to charge balancing processes. Parental magmatic water contents were then calculated for each individual clinopyroxene crystal and subsequently an average was produced for each rock sample.

4.7. Plagioclase-Liquid Hygrometry

In order to obtain an independent and direct estimate for magmatic water contents of the studied lava samples, feldspar and whole-rock compositional data were applied to the plagioclase-liquid hygrometer by *Waters and Lange* [2015], which is an improved version of the previous hygrometer of *Lange et al*. [2009]. The hygrometer is based on plagioclase-liquid exchange between anorthite and albite components. This plagioclase-liquid hygrometer has been calibrated for, and is hence applicable to, a wide range of melt compositions and incorporates calorimetric and volumetric dependencies on pressure and temperature. The estimated error is within ±0.35 wt % H_2O. Feldspar crystallization in basanites of the Western Canary commences at ~1110°C, and increases as temperature decreases to ~1050°C [e.g., *Martì et al*., 2013a]. As an input for the hygrometer we thus assumed a median temperature of 1080°C for the peak of feldspar crystallization. As a pressure input for the hygrometer, we took a pressure range from 700 to 1200 MPa, which is thought to represent the main crystal fractionation level for this magma type on the basis of melt and fluid inclusion studies from La Palma [*Hansteen et al*., 1998; *Nikogosian et al*., 2002].

4.8. Thermobarometry

Whole-rock data, clinopyroxene compositional data, and the derived magmatic water contents from clinopyroxenes were then used to calculate crystallization pressures for the investigated clinopyroxene crystals. We applied thermobarometers that are based on the jadeite-diopside/hedenbergite exchange equilibria between clinopyroxene and coexisting melt [*Putirka et al*., 1996, 2003; *Putirka*, 2008]. Specifically, we used equations (30) and (33) in *Putirka* [2008], which have been shown to be robust under disequilibrium

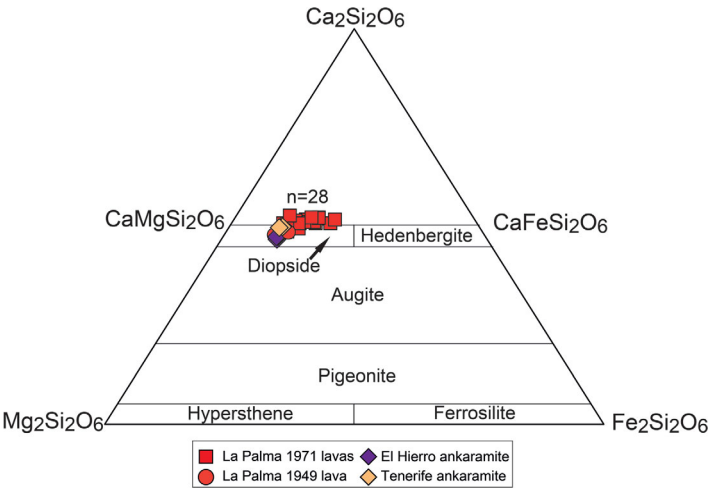

Figure 3. Compositional classification of clinopyroxenes shows the crystals from this study to plot in or close to the diopside field [after *Morimoto et al*., 1988].

conditions [*Mollo et al*., 2010] and have proven reliable in reconstruction of P-T conditions for magmas of a wide compositional range [e.g., *Putirka and Condit*, 2003; *Schwarz et al*., 2004; *Klügel et al*., 2005; *Galipp et al*., 2006; *Longpré et al*., 2008; *Barker et al*., 2009; *Dahren et al*., 2012]. Equilibrium between the crystals and the bulk rock composition of the lava samples has been ascertained using the $K_D(Fe\text{-}Mg)^{cpx\text{-}liq}$ values for Fe-Mg exchange between the melt and the crystals. Crystals in equilibrium with their melt are required to satisfy $K_D(Fe\text{-}Mg)^{cpx\text{-}liq} = 0.28 \pm 0.08$ [see *Putirka*, 2008].

5. Results

5.1. Whole-Rock Geochemistry and Electron Probe Microanalysis

The results for the whole-rock geochemical analysis are listed in Table A2. Unlike the ankaramite samples from El Hierro and Tenerife (n = 2) that plot in the foidite field, the La Palma lavas (n = 8) plot in the basanite field on a total alkali versus silica (TAS) diagram (Figure 2). The clinopyroxene chemical data obtained by EPMA are shown in Table A2. The analyzed clinopyroxenes in this study (n = 28) are titanium-rich diopsides (2.5–3.3 wt % TiO_2) (Table A2 and Figure 3) with Mg numbers between 63 and 80% (mean = 74%). With only very few exceptions, the individual crystals are homogeneous in composition and show limited zonation. Differences in chemical composition between crystals of individual rock samples occur on occasion. The "cations per formula units" for each clinopyroxene crystal are reported in Table A3. The analyzed feldspar crystals are plagioclase (labradorite) with X_{An} between 0.60 and 0.67. Compositional data for feldspar are reported in Table A4.

5.2. FTIR and Rehydration

All analyzed clinopyroxenes showed vibrational bands at 3630, 3530, and 3460 cm^{-1} in the IR spectra (Figure 4), which corresponds to the typical vibrational bands expected for OH in diopside [e.g., *Skogby*, 2006]. The OH band at around 3630 cm^{-1} is prominent when measured along the α and β directions, while the two bands around 3530 and 3460 cm^{-1} dominate along the γ direction. This infrared-pleochroic behavior is typical for clinopyroxene OH bands (Figure 4) [e.g., *Beran*, 1976] and thus excludes the influence of possible OH-bearing impurities. The peaks increased significantly in height in all three directions (α, β, and γ) after thermal annealing in all samples. The biggest increase in peak height was notably always observed for the band at 3630 cm^{-1}. No change in peak positions was observed, however. Water contents corresponding to the spectra differed for the calibrations of *Bell et al*. [1995] and *Libowitzky and Rossman* [1997]. Values determined with the mineral-specific calibration by *Bell et al*. [1995] were about 25% higher, but the authors note that their mineral-specific (augite) calibration is primarily valid for samples with similar OH-spectra. Our diopside spectra are dominated by high-wavenumber bands (3630 cm^{-1}) and thus differ from the spectra presented in *Bell et al*. [1995]. We therefore used the values derived through the calibration by *Libowitzky and Rossman* [1997], which has previously been used successfully for synthetic as well as natural clinopyroxene samples [e.g., *Stalder*, 2004; *Stalder and Ludwig*, 2007; *Sundvall and Stalder*, 2011].

The preannealing water contents calculated from the obtained FTIR spectra for the studied clinopyroxenes vary between rock samples and also within individual lava samples. Most crystals showed water contents between 60 and 100 ppm weight H_2O, but some were completely dry with water contents below the detection limit (<10 ppm). Some crystals, in turn, show substantial water contents of up to 170 ppm (Figure 5

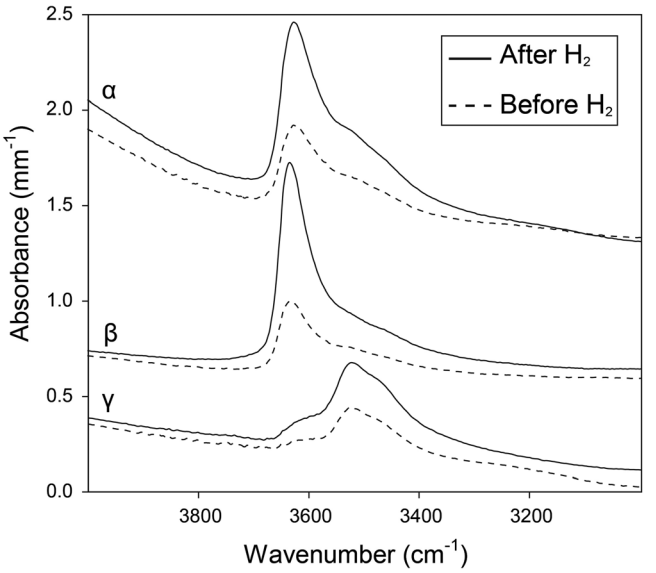

Figure 4. Typical IR-spectra of La Palma clinopyroxene polarized in the α, β, and γ directions. The spectra show the three main vibrational bands of water at 3630, 3530, 3460 cm^{-1}, which are expected for diopside [e.g., *Skogby*, 2006] and relate to different OH-dipole orientations (see text for details). The increase in peak intensity and thus water content after hydrogen treatment is apparent. The spectra shown are from sample LP1971-1(1).

and Table 2). FTIR analysis of the hydrogen-treated crystals reveals water contents between 200 and 420 ppm, with most samples (~86%) falling in the range between 240 and 390 ppm (Figure 5 and Table 2). Significant variation of hydrogen content within individual clinopyroxene crystals has not been observed within the available spatial resolution, but variations can occur between crystals of the same rock sample. Including potential uncertainties from the peak fitting process, such as those involved in the determination of baselines and the absorption calibration, an overall analytical error of ±10% (2 s. d.) is assumed for the determined hydrogen contents in our clinopyroxenes [see *Libowitzky and Rossman*, 1997].

5.3. Mössbauer Spectroscopy

The results for the Mössbauer spectroscopy are shown in Table 3 and a representative spectrum with doublets for Fe^{2+} and Fe^{3+} is shown in Figure 6. On average, the analyzed clinopyroxenes show Fe^{3+}/Fe_{tot} ratios between 37 and 51%. Reduction of ferric iron is observed upon hydrogen treatment (Tables 3 and 4).

5.4. Magmatic Water Contents

Applying the experimentally restored water contents of clinopyroxenes together with the cation-normalized geochemical data and the equation of *O'Leary et al.* [2010], parental magmatic water contents of between 0.84 ± 0.08 and 1.49 ± 0.15 wt % are derived for the La Palma lava samples (n = 8). This is complemented with 1.05 ± 0.10 wt % H_2O for the ankaramite lava sample from El Hierro, and with 0.71 ± 0.07 wt % H_2O for the ankaramite dyke sample from Tenerife. A slight variation of water contents within the 1971 lava samples is expected due to magma differentiation of a common crystallization sequence. All calculated magmatic water contents are summarized in Table 5.

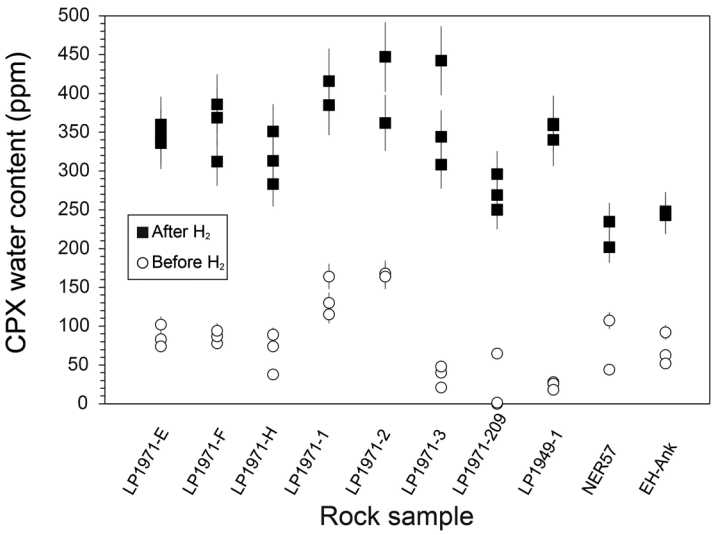

Figure 5. Distribution of measured water contents for clinopyroxene crystals from La Palma, El Hierro, and Tenerife before and after thermal annealing in hydrogen gas. Water contents increase drastically in all samples upon hydrogen treatment.

5.5. Plagioclase/Liquid-Hygrometry

Under the set pressure and temperature conditions for feldspar crystallization in basanite magmas in the Western Canaries (700–1200 MPa; 1080°C) [*Hansteen et al.*, 1998; *Nikogosian et al.*, 2002; *Martí et al.*, 2013b], the plagioclase-liquid hygrometer reveals magmatic water contents between 1.00 ± 0.35 and 1.3 ± 0.35 wt % for the two investigated plagioclase-bearing basanites from La Palma (Table 6).

Table 3. Mössbauer Spectroscopy Results[a]

Sample	int (%)	fwhm (mm/s)	cs (mm/s)	dq (mm/s)	Source
LP1971-E					
Fe^{2+}	57.3	0.35	1.07	2.20	Point
Fe^{3+}	42.7	0.32	0.50	0.63	
LP1971-F					
Fe^{2+}	58.0	0.37	1.06	2.20	Point
Fe^{3+}	42.0	0.34	0.49	0.65	
LP1971-H					
Fe^{2+}	48.8	0.33	1.05	2.24	Point
Fe^{3+}	51.2	0.35	0.47	0.67	
LP1971-1					
Fe^{2+}	58.6	0.32	1.08	2.20	Point
Fe^{3+}	41.4	0.32	0.51	0.67	
LP1971-2					
Fe^{2+}	56.6	0.31	1.06	2.25	Standard
Fe^{3+}	43.4	0.29	0.50	0.67	
LP1971-3					
Fe^{2+}	52.0	0.60	1.06	2.24	Point
Fe^{3+}	48.0	0.57	0.48	0.67	
LP1971-3 (H_2)					
Fe^{2+}	58.8	0.59	1.07	2.24	Point
Fe^{3+}	41.2	0.54	0.51	0.65	
LP1971-209					
Fe^{2+}	54.1	0.57	1.07	2.23	Point
Fe^{3+}	45.9	0.56	0.49	0.64	
LP1971-209 (H_2)					
Fe^{2+}	58.4	0.58	1.07	2.21	Point
Fe^{3+}	41.6	0.54	0.50	0.64	
LP1949-1					
Fe^{2+}	50.6	0.58	1.04	2.25	Standard
Fe^{3+}	49.4	0.56	0.48	0.67	
LP1949-1 (H_2)					
Fe^{2+}	52.2	0.58	1.03	2.22	Standard
Fe^{3+}	47.8	0.53	0.49	0.64	
NER57					
Fe^{2+}	63.1	0.38	1.07	2.16	Standard
Fe^{3+}	36.9	0.29	0.52	0.60	
EH-Ank					
Fe^{2+}	61.9	0.26	1.08	2.17	Standard
Fe^{3+}	38.1	0.23	0.51	0.63	

[a]int, intensity in percentage of total absorption area = Fe^{m+}/Fe_{total}; fwhm, full width at half maximum (including source width); cs, centroid shift; dq, quadrupole splitting. Estimated uncertainty for intensities is ±1%.

The results obtained from the plagioclase-liquid hygrometer serve as an independent test for the validity of our calculated magmatic water contents from clinopyroxenes and the derived thermobarometry results. The magmatic water contents of our basanite samples determined through hydrogen treated clinopyroxene overlap with the range of parental magmatic H_2O contents derived through the feldspar hygrometer (Table 6). This confirms the applicability of our approach using rehydrated clinopyroxenes.

5.6. Thermobarometry

Of the 28 analyzed clinopyroxene crystals, 23 (La Palma n = 18, El Hierro n = 3, Tenerife n = 2) show $K_D(Fe\text{-}Mg)^{cpx\text{-}liq}$ in the range from 0.2 to 0.36 and thus satisfy diopside-hedenbergite exchange equilibria with the bulk rock compositional data (Table 7) [see *Putirka et al.*, 2003]. Using the models of *Putirka* [2008, equations (30) and (33)] and the calculated parental magmatic water contents from the investigated clinopyroxenes, the resulting crystallization pressures and temperatures range from 530 to 970 MPa and from 1120 to 1160°C, respectively. Assuming a combined upper mantle and crustal density of 3100 kg/m^3 [e.g., *Tenzer et al.*, 2013], these crystallization pressures and temperatures correspond to depths of between 16 and 30 km, with the majority of the data clustering around 25 km depth (see Table 7 for details).

6. Discussion

6.1. Clinopyroxene Rehydration and Associated Processes

The variation of hydrogen content between crystals of individual rock samples prior to and after thermal annealing can partly be explained by variation in composition between the crystals (e.g., LP1971-3). However, in some rock samples clinopyroxenes show significant differences in preannealing hydrogen contents (up to 100%, e.g., in LP1971-H) or full dehydration (e.g., in LP1971-209) despite relative compositional homogeneity within and between crystals. Notably, these differences disappear after hydrogen treatment to within the 10% error of FTIR analysis, with the exception of samples showing compositional variations between crystals (Figure 5 and Table 2). We interpret the variation in preannealing hydrogen contents to be a result of various degrees of pre and syneruptive dehydration of our clinopyroxene crystals. If the crystals lost hydrogen by diffusive processes during eruption, then diffusion profiles with higher hydrogen contents toward the crystal interior could be expected [e.g., *Wade et al.*, 2008]. Such diffusion profiles are, however, not observed in our crystals within the available spatial resolution. At expected magmatic temperatures (~1000°C), hydrogen diffusion out of a crystal may occur over distances of mm in time scales of minutes to hours for Fe-rich clinopyroxenes [*Woods et al.*, 2000]. If quenched under such conditions, clinopyroxene crystals may show diffusion profiles [e.g., *Wade et al.*, 2008]. On the other hand, such profiles can be absent in crystals that have undergone slower cooling. Further, upon magma ascent, fluid pressure in the magma is expected to decrease due to degassing [e.g., *Dixon*, 1997; *Dixon et al.*, 1997]. Hydrogen can thus be lost from the clinopyroxene phenocrysts which will equilibrate to the progressively declining fluid pressure by dehydration, following the fast redox

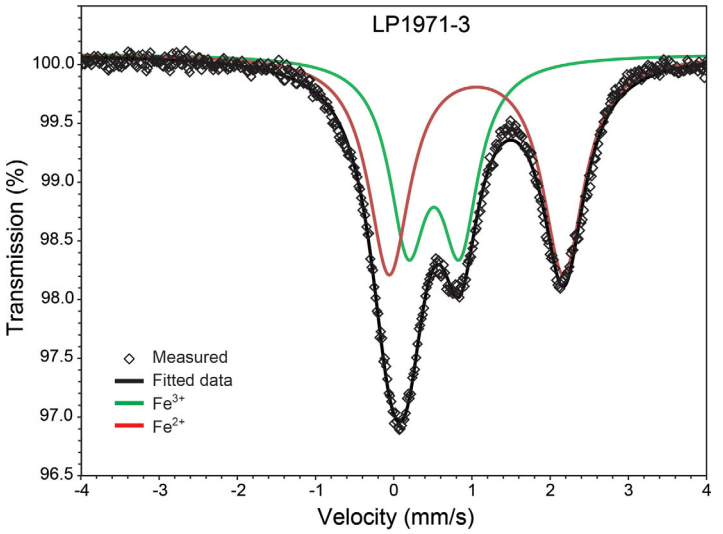

Figure 6. Representative Mössbauer spectrum for clinopyroxene in sample LP1971-3 from La Palma before hydrogen treatment. The spectrum shows the typical Fe^{2+} and Fe^{3+} doublets which were used to determine the concentration of both iron oxidation states in the sample.

reaction (R1). In addition, during eruption at the surface, conditions will become increasingly oxidizing due to exposure to the atmosphere. Upon almost complete degassing of the lava and eventual exposure to the atmosphere, some crystals will have experienced virtually total dehydration. Extensive degassing of our lava samples is furthermore indicated by their highly vesicular appearance. The measured preannealing water contents thus reflect magmatic water contents after partial magma degassing during ascent and during late-stage degassing on eruption.

The results obtained on rehydrated clinopyroxenes show that most crystals reached saturation within 16–32 h of hydrogen treatment at 700°C (Table 2), and no significant changes were observed upon further heating. Mössbauer spectroscopy was used to verify that redox-reaction R1 was active during rehydration and Mössbauer data for the studied samples (LP1971-3, LP1971-209, and LP1949-1) demonstrate reduction of Fe^{3+} to Fe^{2+} after thermal annealing (Table 3). However, the amount of iron in terms of atoms per formula units is much larger than the amount of hydrogen uptake. Therefore, only a minor change in the Fe^{3+}/Fe_{total} ratio is expected, and a precise verification of a 1:1 proportion of the redox reaction is difficult to achieve. The expected decrease in Fe^{3+}/Fe_{total} during rehydration experiments, calculated based on measured incorporation of hydrogen according to R1 into clinopyroxenes from the studied lava samples, varies from 2.1 ± 0.2 to $4.7 \pm 0.5\%$, with an average value of $3.5 \pm 0.3\%$ (Table 4). Measured changes in Fe^{3+}/Fe_{total} for additional crystals from the three investigated lava samples, in turn, range from 1.6 to 6.8%, with an average of 4.2% (Table 4). These deviations largely overlap within the combined analytical error for the Fe^{3+}/Fe_{total} ($\pm 1\%$) and the FTIR analysis ($\pm 10\%$), yet the results indicate that slightly more Fe^{3+} is reduced than hydrogen is incorporated. The cause for these minor discrepancies may lie in the fact that the crystals studied by Mössbauer spectroscopy were powdered during preparation for analysis and so no explicit compositional or hydrogen content analysis could be conducted on these specific crystals. Differences in chemical composition and hydrogen content among crystals were, for example, observed in sample LP1971-3, which also shows the largest deviation in the Mössbauer measurements, implying that compositional and hydrogen variations are indeed the main cause. Notably, similar small deviations from an exact 1:1 relation of the redox reaction (R1) have been observed by previous workers [*Bromiley et al.*, 2004; *Sundvall et al.*, 2009; *Sundvall and Skogby*, 2011].

Moreover, a coupling between clinopyroxene water content and the amount of structural tetrahedral Al^{3+} has previously been identified [*Hauri et al.*, 2006; *Skogby*, 2006; *Wade et al.*, 2008]. The general trend is that with increasing $^{(IV)}Al^{3+}$, the solubility of water in clinopyroxenes increases due to charge balancing processes. This trend is also seen for our samples (Table 5).

Table 4. Changes in Fe_{3+}/Fe_{total} After Rehydration Experiments

Sample	ΔOH (pfu)[a]	Fe_{total} (pfu)	ΔFe^{3+} Expected (%)[b]	ΔFe^{3+} Measured (%)[c]
LP1971-3(1)	0.0072 ± 0.0007	0.2772	2.6 ± 0.3	6.8 ± 2
LP1971-3(2)	0.0078 ± 0.0008	0.2364	3.3 ± 0.3	
LP1971-3(3)	0.0099 ± 0.0010	0.2100	4.7 ± 0.5	
LP1971-209(1)	0.0047 ± 0.0005	0.2260	2.1 ± 0.2	4.3 ± 2
LP1971-209(2)	0.0073 ± 0.0007	0.2223	3.3 ± 0.3	
LP1971-209(3)	0.0067 ± 0.0007	0.2045	3.3 ± 0.3	
LP1949-1(1)	0.0083 ± 0.0008	0.2112	3.9 ± 0.4	1.6 ± 2
LP1949-1(2)	0.0082 ± 0.0008	0.1949	4.2 ± 0.4	
LP1949-1(2)	0.0080 ± 0.0008	0.1837	4.4 ± 0.4	
Average			3.5 ± 0.3	4.2 ± 2

[a]Change in water content per formula unit after hydrogen treatment.
[b]Expected change in Fe_{3+}/Fe_{total} based on hydrogen incorporation.
[c]Measured change in Fe_{3+}/Fe_{total} from Mössbauer spectroscopy. Note: Mössbauer spectroscopy was not carried out on the crystals in first the column.

6.2. P-T Conditions of Clinopyroxenes and Magma Degassing

The calculated crystallization pressures and temperatures for our La Palma, El Hierro, and Tenerife clinopyroxenes overlap with previous temperature and pressure determinations for magma storage under the Western Canaries, based on a range of mineral-melt thermobarometer models as well as melt and fluid inclusion studies [e.g., *Hansteen et al*., 1998; *Nikogosian et al*., 2002; *Klügel et al*., 2005; *Galipp et al*., 2006; *Longpré et al*., 2008; *Stroncik et al*., 2009]. In addition, our data are consistent with seismic unrest data for magma storage at upper mantle depth [e.g., *González et al*., 2013; *Martí et al*., 2013b; *Longpré et al*., 2014]. Indeed, the general model for the Western Canary Islands involves major magma storage reservoirs in the upper mantle at depths between 15 and 30 km that, in turn, feed the mafic (basanitic) volcanic activity at the surface [*Hansteen et al*., 1998; *Klügel et al*., 2000, 2005; *Stroncik et al*., 2009] (Figure 7). The level of crystallization recorded during final equilibration between our clinopyroxene crystals and their parent melts (18–32 km depth) overlaps this established pressure level. It is likely that this level is also where the hydrogen associated structural

Table 5. Water Contents of Magmas in the Western Canary Archipelago[a]

Sample	$^{(IV)}Al^{3+}$	$[H_2O]_{cpx}$ After H_2 Treatment (ppm)[b]	Ca^{2+}	$lnD_{(cpx\text{-}melt)}$	$D_{(cpx\text{-}melt)}$	$[H_2O]_{Melt}$ (wt %)	Average $[H_2O]_{Melt}$ (wt %)
La Palma							
LP1971-E(1)	0.228	360	0.913	−3.630	0.027	1.36 ± 0.14	1.12 ± 0.11
LP1971-E(2)	0.272	336	0.901	−3.336	0.036	0.94 ± 0.09	
LP1971-E(3)	0.270	365	0.916	−3.363	0.035	1.05 ± 0.11	
LP1971-F(1)	0.210	347	0.903	−3.739	0.024	1.46 ± 0.15	1.46 ± 0.15
LP1971-F(2)	0.195	312	0.906	−3.840	0.021	1.45 ± 0.15	
LP1971-F(3)	0.227	386	0.908	−3.633	0.026	1.46 ± 0.15	
LP1971-H(1)	0.244	282	0.908	−3.524	0.029	0.96 ± 0.10	1.04 ± 0.10
LP1971-H(2)	0.249	351	0.901	−3.480	0.031	1.14 ± 0.11	
LP1971-H(3)	0.251	313	0.906	−3.475	0.031	1.01 ± 0.10	
LP1971-1(1)	0.249	385	0.911	−3.489	0.031	1.26 ± 0.13	1.35 ± 0.14
LP1971-1(2)	0.252	416	0.889	−3.451	0.032	1.31 ± 0.13	
LP1971-1(3)	0.222	385	0.898	−3.655	0.026	1.49 ± 0.15	
LP1971-2(1)	0.271	360	0.891	−3.331	0.036	1.01 ± 0.10	1.01 ± 0.10
LP1971-2(2)	0.306	447	0.898	−3.111	0.045	1.00 ± 0.10	
LP1971-3(1)	0.268	308	0.914	−3.369	0.034	0.89 ± 0.09	0.87 ± 0.08
LP1971-3(2)	0.284	344	0.911	−3.266	0.038	0.90 ± 0.09	
LP1971-3(3)	0.341	442	0.914	−2.770	0.063	0.80 ± 0.08	
LP1971-209(1)	0.257	250	0.904	−3.431	0.032	0.77 ± 0.08	0.84 ± 0.08
LP1971-209(2)	0.250	296	0.914	−3.486	0.031	0.97 ± 0.10	
LP1971-209(3)	0.273	269	0.933	−3.357	0.035	0.77 ± 0.08	
LP1949-1(1)	0.232	390	0.901	−3.594	0.027	1.42 ± 0.14	1.49 ± 0.15
LP1949-1(2)	0.209	363	0.917	−3.760	0.023	1.56 ± 0.16	
LP1949-1(3)	0.204	340	0.908	−3.781	0.023	1.49 ± 0.15	
Tenerife							
NER57(1)	0.258	235	0.931	−3.457	0.032	0.75 ± 0.08	0.71 ± 0.07
NER57(2)	0.251	202	0.936	−3.503	0.030	0.67 ± 0.07	
El Hierro							
EH-Ank(1)	0.205	249	0.878	−3.743	0.024	1.05 ± 0.11	1.05 ± 0.10
EH-Ank(2)	0.208	245	0.903	−3.750	0.024	1.04 ± 0.10	
EH-Ank(3)	0.206	243	0.898	−3.760	0.023	1.04 ± 0.10	

[a]Calculated uncertainties (2 s.d.) for $^{(IV)}Al^{3+}$ and Ca^{2+} are ±0.010 and ±0.007 for $D_{(cpx\text{-}melt)}$. Estimated uncertainties for water contents are ±10% for cpx and magmas.
[b]Average value for saturated cpx crystals.

Table 6. Feldspar/Liquid Hygrometry Results

Sample	X_{An}	X_{Ab}	X_{Or}	Temperature (°C)[a]	Pressure (MPa)[a]	H_2O (wt %)	Pressure (MPa)[a]	H_2O (wt %)
LP1971-1	0.61	0.37	0.02	1080	700	1.2 ± 0.35	1200	1.3 ± 0.35
LP1971-1	0.66	0.33	0.02	1080	700	1.2 ± 0.35	1200	1.3 ± 0.35
LP1971-1	0.63	0.35	0.02	1080	700	1.2 ± 0.35	1200	1.3 ± 0.35
LP1971-1	0.67	0.31	0.02	1080	700	1.3 ± 0.35	1200	1.3 ± 0.35
LP1971-1	0.66	0.33	0.02	1080	700	1.2 ± 0.35	1200	1.3 ± 0.35
LP1971-1	0.64	0.34	0.02	1080	700	1.2 ± 0.35	1200	1.3 ± 0.35
LP1971-1	0.66	0.33	0.02	1080	700	1.2 ± 0.35	1200	1.3 ± 0.35
LP1971-1	0.61	0.37	0.02	1080	700	1.2 ± 0.35	1200	1.3 ± 0.35
LP1971-1	0.61	0.39	0.00	1080	700	1.2 ± 0.35	1200	1.2 ± 0.35
LP1971-F	0.63	0.35	0.02	1080	700	1.0 ± 0.35	1200	1.0 ± 0.35

[a]Pressures and temperature for main level of feldspar crystallization based on *Hansteen et al*. [1998], *Nikogosian et al*. [2002], and *Martì et al*. [2013a].

defects within the crystals were generated. In addition to the main upper mantle reservoirs, magma ascending underneath the Western Canary Islands also passes through two shallower storage levels, namely the "magma underplating zone," between 10 and 15 km depth, and the "intrusive core complex," at 5–10 km depth (Figure 7). However, residence times for the mafic magmas at these levels have been found to be too short to cause significant re-equilibration between the crystals and their melt [*Hansteen et al*., 1998; *Klügel et al*., 2000, 2005; *Stroncik et al*., 2009] and hence no resetting of structural defects is thought to occur. In combination with our calculated crystallization pressures, the presented parental magmatic water contents thus correspond to the deeper mantle reservoir, where degassing of juvenile Canary Island magmas usually commences [e.g., *Hansteen et al*., 1998]. Our rehydrated clinopyroxenes and the corresponding calculated magmatic water contents thus provide complementary evidence for magma storage within the main upper mantle reservoir. Our results are likely a close approximation of the water contents of mafic Western Canary magmas at this depth.

Table 7. Thermobarometry Results[a]

Sample	Pressure (MPa)	Temperature (°C)	Depth (km)	$K_D(Fe\text{-}Mg)^{cpx\text{-}liq}$[b]
La Palma				
LP1971-E(1)	845	1144	26	0.29
LP1971-F(1)	730	1140	23	0.26
LP1971-F(3)	782	1142	24	0.28
LP1971-H(1)	715	1145	22	0.30
LP1971-H(3)	970	1157	30	0.36
LP1971-1(1)	858	1150	27	0.31
LP1971-1(2)	800	1156	25	0.28
LP1971-1(3)	788	1148	24	0.28
LP1971-2(1)	840	1167	26	0.25
LP1971-2(2)	903	1166	28	0.33
LP1971-3(1)	912	1157	28	0.36
LP1971-3(2)	792	1152	25	0.30
LP1971-209(1)	820	1159	25	0.27
LP1971-209(2)	658	1140	20	0.27
LP1971-209(3)	527	1124	16	0.25
LP1949-1(1)	753	1144	23	0.25
LP1949-1(2)	695	1128	22	0.22
LP1949-1(3)	568	1125	18	0.20
Tenerife				
NER57(1)	648	1139	20	0.25
NER57(2)	550	1132	17	0.25
El Hierro				
EH-Ank(1)	768	1159	24	0.24
EH-Ank(2)	659	1141	20	0.23
EH-Ank(3)	692	1145	21	0.24

[a]Errors for pressure and temperature are ±170 MPa and ±42°C, respectively.
[b]Equilibrium for $K_D(Fe\text{-}Mg)^{cpx\text{-}liq} = 0.28 \pm 0.08$.

6.3. Calculated Parental Magma H_2O Contents in a Regional and Global Context

We first note that the calculated water contents for magmas from La Palma agree with the results from feldspar hygrometry for these samples. Moreover, our data from La Palma, El Hierro, and Tenerife overlap with the range of previously determined water contents for mafic rocks from the Canary Islands and from other ocean island suites [e.g., *Moore*, 1970; *Dixon et al*., 1997; *Wallace*, 1998; *Gurenko and Schmincke*, 2000; *Dixon and Clague*, 2001; *Longpré et al*., 2009; *Deegan et al*., 2012] (Figure 8a).

Basanite lavas from La Palma and the El Hierro ankaramite sample show an average water content of 1.13 ± 0.11 wt %. This value overlaps with the average value of 1.08 ± 0.11 wt % for alkali basalt glasses from Gran Canaria [*Wallace*, 1998]. The magmatic water content of 0.71 ± 0.07 wt % determined for the ankaramite dyke sample from Tenerife overlaps within error with the average value of 0.63 ± 0.13 wt % H_2O determined by *Deegan et al*. [2012] for the ankaramite suite of Tenerife's Northeast rift zone. In conjunction with the available

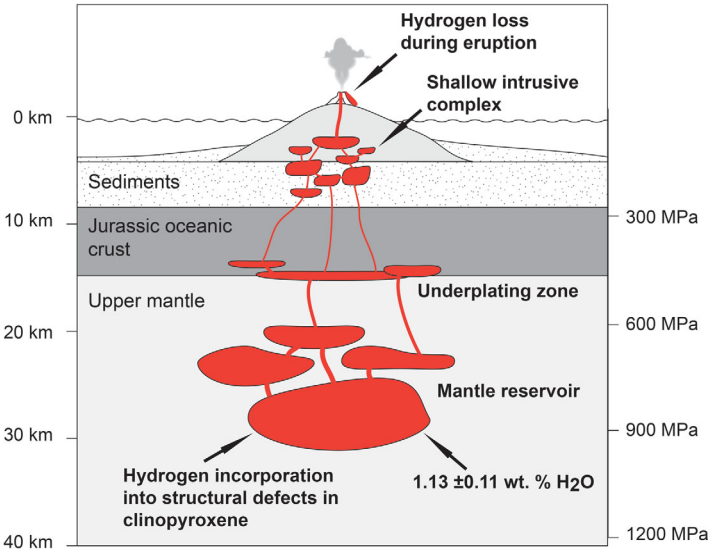

Figure 7. Simplified sketch of the magma plumbing systems underneath La Palma and El Hierro based on models by *Hansteen et al.* [1998], *Klügel et al.* [2000, 2005], and *Stroncik et al.* [2009]. Clinopyroxene grew dominantly at a depth of 20–30 km, implying that hydrogen incorporation into clinopyroxene structural defects occurred in the main mantle reservoir. Residence times of ascending magmas in the shallower underplating zone and intrusive core complex are too short to cause any significant defect resetting coupled to cation diffusion [e.g., *Hansteen et al.*, 1998; *Klügel et al.*, 2005]. Hydrogen loss from clinopyroxene occurs during ascent and upon eruption of the lava (see text for details).

geochemical data from, e.g., Gran Canaria and Tenerife [*Wallace*, 1998; *Gurenko and Schmincke*, 2000; *Deegan et al.*, 2012], our results from the Western Canaries increase the density of available data in a broader compilation of magmatic H_2O and K_2O for the Canaries and other ocean island systems. In fact, our data bridge a previous "gap" in the available Canary Island data set, because magmas that connect medium and high primary H_2O and K_2O contents within the available data suite have thus far not been documented (Figure 8b).

The basanites from La Palma and the ankaramite from El Hierro (average 1.13 ± 0.11 wt % H_2O) further overlap with, or are close to, the average water contents of 0.99 ± 0.10 wt % and 0.76 ± 0.08 wt % for alkali ocean island basalt and basanite glasses from Hawaii and the average value of 0.90 ± 0.28 wt % H_2O proposed for alkali ocean island basalts of the Revilagigedo Islands [*Moore*, 1970; *Dixon et al.*, 1997; *Dixon and Clague*, 2001]. In addition, the obtained results for the Western Canaries correlate with data presented by *Kovalenko et al.* [2007] who classified three different types of globally available ocean island melts. According to their scheme, our data fall into the type III melt group that is defined as having K_2O wt % > 0.20 wt %, an average water content of 0.62 ± 0.30 wt % H_2O, but a minimum H_2O content of 0.20 wt %. This melt type is considered to be dominant in the Canary archipelago by these authors [*Kovalenko et al.*, 2007].

Our results therefore reproduce the established H_2O range of mafic ocean island magmas from the Canary Islands, as well as global ocean island systems, and hence complement the currently available data for Canary magmatic water contents [cf., *Wallace*, 1998; *Gurenko and Schmincke*, 2000; *Kovalenko et al.*, 2007; *Deegan et al.*, 2012].

7. Conclusions

We have presented parental magmatic water contents for lavas from the Western Canary islands which were derived using rehydrated structural defects in clinopyroxene. We found that the resulting data are consistent with magmatic H_2O contents derived through feldspar-liquid hygrometry for the same samples and with H_2O data from the Canary Islands and ocean island basalts globally determined in previous studies and through a variety of established methods. This realization supports the premise that, depending on eruption style, clinopyroxene crystals may dehydrate upon magma ascent and during eruption. The initial water contents of crystals at their crystallization levels can, however, be restored experimentally by hydrogen treatment. Equilibrium H_2O contents of the parental magma can then be established through the

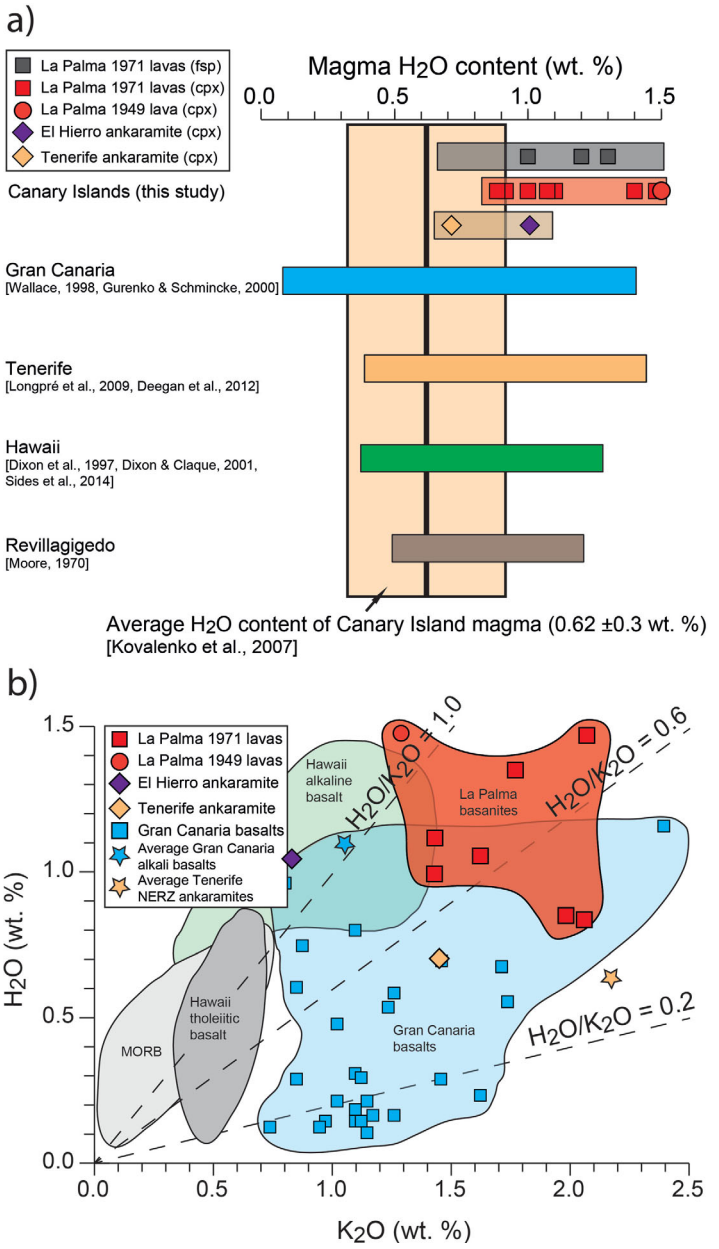

Figure 8. (a) Distribution of magmatic water contents determined through feldspar-liquid hygrometry and rehydrated clinopyroxenes for Western Canary magmas (based on data from Tables 5 and 6) in comparison with other studies performed on Gran Canaria [*Wallace*, 1998; *Gurenko and Schmincke*, 2000], Tenerife [*Deegan et al*., 2012], Hawaii [*Dixon et al*., 1997; *Dixon and Claque*, 2001], and Revillagigedo [*Moore*, 1970]. The values obtained for the Western Canary islands through the water contents in clinopyroxene crystals overlap with the available data from Tenerife and Gran Canaria and with other ocean island suites obtained by different methods. (b) Comparison of H_2O and whole-rock K_2O contents for the La Palma lavas to data from Gran Canaria and the Northeast rift zone (NERZ) on Tenerife [data from *Gurenko and Schmincke*, 2000; *Hoernle and Schmincke*, 1993b; *Gurenko et al*., 1996; *Wallace*, 1998; *Deegan et al*., 2012]. Stars represent average values for glass inclusions in alkali basalts from Gran Canaria [after *Hoernle and Schmincke*, 1993b; *Gurenko et al*., 1996; *Wallace*, 1998] and bulk rock data for the Northeast rift zone [*Deegan et al*., 2012]. Data presented in this study complement available data for the Canary Islands by widening the recorded field and bridging a previous compositional gap toward higher H_2O and K_2O contents in the Canary Island data set.

equation of, e.g., *O'Leary et al*. [2010] that allows us to calculate distribution coefficients between clinopyroxene and basaltic melts. The method for determining magmatic water contents outlined in this study may provide a useful complement to existing approaches, especially for mafic ocean island suites (e.g., nephelinites, basanites, and ankaramites) where clinopyroxene is frequently found as a main mineral phase in erupted products.

Appendix A

Below we provide whole rock chemical compositions of rock samples used in this study (Table A1). Major elements of clinopyroxenes from this study are presented in Table A2 and normalized cations per formula units are presented in Table A3. Major elements and mineral mole fractions of feldspars analyzed in this study are summarized in Table A4. For detailed information on data acquisition please see the method section in the main text.

Table A1. Whole-Rock Chemical Compositions of Rock Samples Used in This Study[a]

Sample	SiO_2	Al_2O_3	Fe_2O_3	MgO	CaO	Na_2O	K_2O	TiO_2	P_2O_5	MnO	Cr_2O_3	Total
LP1971-E	43.40	13.76	13.68	8.09	10.97	3.71	1.43	3.71	0.82	0.20	0.03	99.80
LP1971-F	43.80	15.14	12.79	6.45	10.20	4.41	2.07	3.81	0.87	0.21	0.02	99.77
LP1971-H	43.17	12.91	13.20	8.36	11.71	3.61	1.62	3.79	0.94	0.20	0.04	99.55
LP1971-1	44.56	15.05	12.78	6.00	10.19	4.39	1.77	3.72	0.93	0.20	0.01	99.60
LP1971-2	43.32	13.75	13.57	8.18	11.00	3.67	1.43	3.66	0.81	0.20	0.03	99.62
LP1971-3	43.46	14.95	12.88	6.55	10.27	4.31	2.06	3.76	0.88	0.21	0.02	99.35
LP1971-209	43.51	15.18	12.74	6.19	10.20	4.53	1.98	3.83	0.88	0.21	0.01	99.26
LP1949	44.31	13.92	13.35	8.15	10.97	3.60	1.29	3.39	0.69	0.20	0.04	99.92
EH-Ank	40.24	8.76	17.78	13.39	11.46	2.00	0.83	5.03	0.42	0.19	0.08	100.18
NER57[b]	40.12	13.99	16.13	6.56	11.87	3.31	1.45	5.04	0.79	0.17	n.d.[c]	99.43

[a]Major elements are given as wt % oxide.
[b]Values taken from *Deegan et al*. [2012].
[c]n.d.: not determined.

Table A2. Major Elements of Western Canary Clinopyroxenes Obtained by Electron Probe Micro Analysis (EPMA)[a]

Sample	SiO_2	Al_2O_3	MgO	Na_2O	MnO	TiO_2	K_2O	CaO	FeO	Cr_2O_3	Total
LP1971-E(1)	47.34	6.18	12.05	0.76	0.19	2.44	0.01	22.76	7.53	0.15	99.41
LP1971-E(2)	45.64	7.39	9.93	1.03	0.24	2.71	0.01	22.21	10.06	0.02	99.23
LP1971-E(3)	45.94	7.26	10.6	0.86	0.18	2.63	0.01	22.69	8.78	0.07	99.27
LP1971-F(1)	47.82	5.71	12.84	0.60	0.11	2.44	0.01	22.52	7.06	0.04	99.13
LP1971-F(2)	48.10	5.36	11.17	1.10	0.17	2.20	0.00	22.53	8.89	0.01	99.54
LP1971-F(3)	47.42	6.25	12.40	0.66	0.17	2.48	0.01	22.67	7.31	0.02	99.38
LP1971-H(1)	46.73	6.43	12.14	0.59	0.13	2.89	0.02	22.54	7.64	0.03	99.13
LP1971-H(2)	46.28	6.84	10.26	0.96	0.29	2.35	0.01	22.24	10.04	0.00	99.26
LP1971-H(3)	47.62	6.04	11.20	0.98	0.19	2.33	0.01	22.55	8.72	0.01	99.63
LP1971-1(1)	46.80	6.63	11.95	0.75	0.18	2.70	0.00	22.73	7.77	0.03	99.55
LP1971-1(2)	46.83	7.11	12.49	0.61	0.14	2.55	0.01	22.22	7.38	0.15	99.50
LP1971-1(3)	47.76	6.27	12.65	0.63	0.14	2.19	0.01	22.52	7.50	0.06	99.73
LP1971-2(1)	46.60	7.36	13.18	0.64	0.10	2.22	0.04	22.41	6.93	0.03	100.27
LP1971-2(2)	45.07	8.23	11.40	0.73	0.11	3.31	0.01	22.29	8.05	0.01	99.21
LP1971-3(1)	45.87	7.28	10.85	0.83	0.06	2.77	0.00	22.60	8.78	0.02	99.08
LP1971-3(2)	45.83	7.48	11.84	0.67	0.17	3.23	0.01	22.70	7.55	0.00	99.49
LP1971-3(3)	44.56	8.56	10.38	0.94	0.24	3.32	0.01	22.75	9.14	0.01	99.90
LP1971-209	46.42	6.91	12.34	0.68	0.14	2.72	0.00	22.47	7.20	0.01	98.89
LP1971-209(2)	46.95	6.73	12.56	0.55	0.10	2.77	0.00	22.88	7.14	0.02	99.69
LP1971-209(3)	46.07	7.30	12.35	0.48	0.06	2.99	0.01	23.23	6.53	0.06	99.08
LP1949-1(1)	47.50	6.67	12.76	0.61	0.08	2.50	0.00	22.59	6.79	0.07	99.58
LP1949-1(2)	48.29	5.69	13.22	0.61	0.12	2.45	0.01	23.08	6.28	0.02	99.76
LP1949-1(3)	48.18	5.56	13.66	0.47	0.09	2.30	0.00	22.75	5.89	0.27	99.17
EH-Ank(1)	48.31	5.64	13.58	0.59	0.10	2.36	0.01	22.06	6.87	0.10	99.62
EH-Ank (2)	48.03	5.48	13.35	0.55	0.10	2.52	0.00	22.60	6.62	0.05	99.31
EH-Ank (3)	48.09	5.62	13.30	0.56	0.08	2.43	0.01	22.47	6.66	0.05	99.27
NER57(1)	46.53	6.58	12.60	0.48	0.12	3.29	0.00	23.20	6.41	0.02	99.23
NER57(2)	46.57	6.15	12.98	0.42	0.08	3.15	0.00	23.27	6.19	0.01	98.82

[a]Major elements are given as wt % oxide.

Table A3. Normalized Cations per Formula Unit of Major Elements in Western Canary Clinopyroxenes

Sample	Si^{4+}	Al^{3+}	Mg^{2+}	Na^{+}	Mn^{2+}	Ti^{4+}	K^{+}	Ca^{2+}	Fe^{2+a}	Fe^{3+a}	Cr^{3+}	Total
LP1971-E(1)	1.772	0.273	0.673	0.055	0.006	0.069	0.000	0.913	0.135	0.101	0.005	4.000
LP1971-E(2)	1.728	0.330	0.560	0.076	0.008	0.077	0.001	0.901	0.183	0.136	0.001	4.000
LP1971-E(3)	1.730	0.322	0.610	0.063	0.006	0.075	0.000	0.916	0.158	0.118	0.002	4.000
LP1971-F(1)	1.790	0.252	0.717	0.043	0.003	0.069	0.001	0.903	0.128	0.093	0.001	4.000

Table A3. (continued)

Sample	Si^{4+}	Al^{3+}	Mg^{2+}	Na^{+}	Mn^{2+}	Ti^{4+}	K^{+}	Ca^{2+}	Fe^{2+a}	Fe^{3+a}	Cr^{3+}	Total
LP1971-F(2)	1.805	0.237	0.625	0.080	0.006	0.062	0.000	0.906	0.162	0.117	0.000	4.000
LP1971-F(3)	1.773	0.275	0.691	0.048	0.005	0.070	0.000	0.908	0.133	0.096	0.001	4.000
LP1971-H(1)	1.756	0.285	0.680	0.043	0.004	0.082	0.001	0.908	0.117	0.123	0.001	4.000
LP1971-H(2)	1.751	0.305	0.579	0.071	0.009	0.067	0.000	0.901	0.155	0.163	0.000	4.000
LP1971-H(3)	1.785	0.267	0.626	0.071	0.006	0.066	0.000	0.906	0.133	0.140	0.000	4.000
LP1971-1(1)	1.751	0.292	0.666	0.054	0.006	0.076	0.000	0.911	0.142	0.101	0.001	4.000
LP1971-1(2)	1.748	0.313	0.695	0.044	0.004	0.072	0.000	0.889	0.135	0.095	0.005	4.000
LP1971-1(3)	1.778	0.275	0.702	0.045	0.005	0.061	0.000	0.898	0.137	0.097	0.002	4.000
LP1971-2(1)	1.729	0.322	0.729	0.046	0.003	0.062	0.002	0.891	0.122	0.093	0.001	4.000
LP1971-2(2)	1.694	0.365	0.639	0.053	0.004	0.094	0.000	0.898	0.143	0.110	0.000	4.000
LP1971-3(1)	1.732	0.324	0.611	0.061	0.002	0.079	0.000	0.914	0.160	0.117	0.001	4.000
LP1971-3(2)	1.716	0.330	0.661	0.049	0.005	0.091	0.001	0.911	0.137	0.100	0.000	4.000
LP1971-3(3)	1.671	0.378	0.580	0.069	0.008	0.094	0.000	0.914	0.149	0.137	0.000	4.000
LP1971-209(1)	1.743	0.306	0.691	0.050	0.004	0.077	0.000	0.904	0.120	0.106	0.000	4.000
LP1971-209(2)	1.750	0.296	0.698	0.040	0.003	0.078	0.000	0.914	0.118	0.104	0.001	4.000
LP1971-209(3)	1.727	0.323	0.690	0.035	0.002	0.084	0.000	0.933	0.109	0.096	0.002	4.000
LP1949-1(1)	1.768	0.293	0.708	0.044	0.003	0.070	0.000	0.901	0.107	0.105	0.002	4.000
LP1949-1(2)	1.791	0.249	0.731	0.044	0.004	0.068	0.000	0.917	0.099	0.096	0.001	4.000
LP1949-1(3)	1.796	0.244	0.759	0.034	0.003	0.064	0.000	0.908	0.093	0.091	0.008	4.000
EH-Ank(1)	1.795	0.247	0.752	0.042	0.003	0.066	0.000	0.878	0.132	0.081	0.003	4.000
EH-Ank(2)	1.792	0.241	0.742	0.039	0.003	0.071	0.000	0.903	0.128	0.079	0.001	4.000
EH-Ank(3)	1.794	0.247	0.740	0.041	0.003	0.068	0.000	0.898	0.129	0.079	0.002	4.000
NER57(1)	1.742	0.290	0.703	0.035	0.004	0.093	0.000	0.931	0.127	0.074	0.001	4.000
NER57(2)	1.749	0.272	0.726	0.031	0.003	0.089	0.000	0.936	0.123	0.072	0.000	4.000

[a]Values calculated using data obtained from Mössbauer analysis before hydrogen treatment.

Table A4. Major Elements of Western Canary Feldspars Obtained by Electron Probe Micro Analysis (EPMA)[a]

Sample	SiO_2	Al_2O_3	MgO	Na_2O	MnO	TiO_2	K_2O	CaO	FeO	Cr_2O_3	Total	X_{An}	X_{Ab}	X_{Or}
LP1971-1	52.72	29.84	0.09	4.13	0.01	0.18	0.30	12.30	0.70	0.02	100.28	0.61	0.37	0.02
LP1971-1	51.80	30.90	0.10	3.63	0.00	0.16	0.29	13.20	0.83	0.00	100.91	0.66	0.33	0.02
LP1971-1	52.27	30.25	0.08	3.81	0.05	0.14	0.32	12.53	0.71	0.01	100.16	0.63	0.35	0.02
LP1971-1	51.33	31.15	0.11	3.42	0.00	0.18	0.28	13.25	0.93	0.00	100.65	0.67	0.31	0.02
LP1971-1	51.87	30.83	0.12	3.60	0.03	0.09	0.26	13.16	0.66	0.00	100.62	0.66	0.33	0.02
LP1971-1	52.50	30.24	0.11	3.70	0.00	0.25	0.32	12.55	0.83	0.02	100.51	0.64	0.34	0.02
LP1971-1	51.82	30.50	0.12	3.58	0.00	0.27	0.27	13.02	1.03	0.00	100.61	0.66	0.33	0.02
LP1971-1	52.94	29.84	0.10	4.08	0.04	0.20	0.27	12.08	0.77	0.00	100.32	0.61	0.37	0.02
LP1971-1	53.05	30.02	0.04	4.33	0.00	0.02	0.08	12.23	0.22	0.01	100.01	0.61	0.39	0.00
LP1971-F	52.57	29.23	0.13	3.88	0.06	0.16	0.30	12.68	1.10	0.00	100.11	0.63	0.35	0.02

[a]Major elements are given as wt % oxide.

Acknowledgments
We thank Kirsten Zaczek and Juan Carlos Carracedo for help during sample collection and Lisa Samrock, Soophie Omidian, and Per-Olof Persson for help with sample preparation. Abigail K. Barker is acknowledged for providing the feldspar compositional data. We also thank Laura E. Waters and Rebecca A. Lange for kindly providing the latest version of their feldspar-liquid hygrometer. Further, we thank Jeremy Bellucci and the two anonymous reviewers for their comments, which helped to improve this manuscript. Generous financial support for this project was provided by the Swedish Research Council and the Royal Swedish Academy of Sciences. The data for this paper are available in the text, tables, and references therein and from the corresponding author on request.

References

Abaud, C., E. H. Hauri, and M. M. Hirschmann (2004), Hydrogen partition coefficients between nominally anhydrous minerals and basaltic melts, *Geophys. Res. Lett.*, *31*, L20611, doi:10.1029/2004GL021341.

Abdel-Monem, A., N. D. Watkins, and P. W. Gast (1972), K/Ar ages; volcanic stratigraphy and geomagnetic polarity history of Tenerife, La Palma and El Hierro, *Am. J. Sci.*, *272*, 805–825.

Ancochea, E., J. M. Fúster, E. Ibarrola, A. Cendrero, J. Coello, F. Hernán, J. M. Cantagrel, and C. Jamond (1990), Volcanic evolution of the Island of Tenerife (Canary Islands) in the light of new K-Ar data, *J. Volcanol. Geotherm. Res.*, *44*, 231–249.

Anguita, F., and F. Hernán (1975), A propagating fracture model versus a hot-spot origin for the Canary Islands, *Earth Planet. Sci. Lett.*, *27*, 11–19, doi:10.1016/0012-821X(75)90155-7.

Anguita, F., and F. Hernán (2000), The Canary Islands origin: A unifying model, *J. Volcanol. Geotherm. Res.*, *103*, 1–26, doi:10.1016/S0377-0273(00)00195-5.

Araña, V., and E. Ibarrola (1973), Rhyolitic pumice in the basaltic pyroclasts from the 1971 eruption of Teneguía volcano, Canary Islands, *Lithos*, *6*, 273–278, doi:10.1016/0024-4937(73)90088-1.

Baker, D. R. (2008), The fidelity of melt inclusions as records of melt composition, *Contrib. Mineral. Petrol.*, *156*, 357–395, doi:10.1007/s00410-008-0291-3.

Barker, A. K., P. M. Holm, D. W. Peate, and J. A. Baker (2009), Geochemical stratigraphy of submarine lavas (3–5 Ma) from the Flamengos Valley, Santiago, Southern Cape Verde Islands, *J. Petrol.*, *50*, 169–193, doi:10.1093/petrology/egn081.

Belkin, H. E., B. De Vivo, K. Török, and J. D. Webster (1998), Pre-eruptive volatile content, melt-inclusion chemistry, and microthermometry of interplinian Vesuvius lavas (pre-A.D. 1631), *J. Volcanol. Geotherm. Res.*, *82*, 79–95, doi:10.1016/S0377-0273(97)00058-9.

Bell, D. R., P. D. Ihinger, and G. R. Rossman (1995), Quantitative analysis of trace OH in garnet and pyroxenes, *Am. Mineral.*, *80*, 465–474.

Beran, A. (1976), Messung des Ultrarot-Pleochroismus von Mineralen. XIV. Der Pleochroismus der OH-Streckfrequenz in Diopsid, *Tschermaks Mineral. Petrogr. Mitt.*, *23*, 79–85.

Bosshard, E., and D. J. Macfarlane (1970), Crustal structure of the western Canary Islands from seismic refraction and gravity data, *J. Geophys. Res.*, *75*, 4901–4918, doi:10.1029/JB075i026p04901.
Bromiley, G. D., H. Keppler, C. McCammon, F. A. Bromiley, and S. D. Jacobsen (2004), Hydrogen solubility and speciation in natural, gemquality chromian diopside, *Am. Mineral.*, *89*, 941–949.
Carracedo, J. C., and V. R. Troll (Eds.) (2013), *Teide Volcano: Geology and Eruptions of a Highly Differentiated Oceanic Stratovolcano, Active Volcanoes of the World*, vol. 1, Springer, Heidelberg, Germany.
Carracedo, J. C., S. Day, H. Guillou, E. Rodríguez Badiola, J. A. Canas, and F. J. Pérez Torrado (1998), Hotspot volcanism close to a passive continental margin: The Canary Islands, *Geol. Mag.*, *135*, 591–604.
Carracedo, J. C., E. R. Badiola, H. Guillou, J. de La Nuez, and F. J. Pérez Torrado (2001), Geology and volcanology of La Palma and El Hierro, Western Canaries, *Estud. Geol.*, *57*, 175–273.
Carracedo, J. C., H. Guillou, S. Nomade, E. Rodríguez Badiola, R. Paris, V. R. Troll, S. Wiesmaier, A. Delcamp, and J. L. Fernández-Turiel (2011), Evolution of ocean-island rifts: The Northeast rift zone of Tenerife, Canary Islands, *Geol. Soc. Am. Bull.*, *123*, 562–584.
Cashman, K. V. (2004), Volatile controls on magma ascent and eruption, in *The State of the Planet: Frontiers and Challenges in Geophysics*, edited by R. S. J. Sparks and C. J. Hawkesworth, AGU, Washington, D. C., doi:10.1029/150GM10.
Cherniak, D. J., and A. Dimanov (2010), Diffusion in pyroxene, mica and amphibole, *Rev. Mineral. Geochem.*, *72*, 641–690.
Dahren, B., V. R. Troll, U. B. Andersson, J. P. Chadwick, M. F. Gardner, K. Jaxybulatov, and I. Koulakov (2012), Magma plumbing beneath Anak Krakatau volcano, Indonesia: Evidence for multiple magma storage regions, *Contrib. Mineral. Petrol.*, *163*(4), 631–651, doi:10.1007/s00410-011-0690-8.
Deegan, F. M., V. R. Troll, A. K. Barker, C. Harris, J. P. Chadwick, J. C. Carracedo, and A. Delcamp (2012), Crustal versus source processes recorded in dykes from the Northeast volcanic rift zone of Tenerife, Canary Islands, *Chem. Geol.*, *334*, 324–344, doi:10.1016/j.chemgeo.2012.10.013.
Delcamp, A., M. S. Petronis, V. R. Troll, J. C. Carracedo, B. van Wyk de Vries, and F. J. Perez-Torrado (2010), Vertical axis rotation of the upper portions of the North-East rift of Tenerife Island inferred from paleomagnetic data, *Tectonophysics*, *492*, 40–59.
Delcamp, A., V. R. Troll, B. van Wyk de Vries, J. C. Carracedo, M. S. Petronis, F. J. Pérez-Torrado, and F. M. Deegan (2012), Dykes and structures of the NE-rift of Tenerife, Canary Islands: A record of stabilisation and destabilisation of ocean island rift-zones, *Bull. Volcanol.*, *74*, 963–980, doi:10.1007/s00445-012-0577-1.
Dingwell, D. B. (1996), Volcanic dilemma-flow or blow?, *Science*, *23*, 1054–1055, doi:10.1126/science.273.5278.1054.
Dixon, J. E. (1997), Degassing of alkalic basalts, *Am. Mineral.*, *82*, 368–378.
Dixon, J. E., and D. A. Clague (2001), Volatiles in basaltic glasses from Loihi Seamount, Hawaii: Evidence for a relatively dry plume component, *J. Petrol.*, *42*, 627–654, doi:10.1093/petrology/42.3.627.
Dixon, J. E., D. A. Clague, P. Wallace and R. Poreda (1997), Volatiles in alkalic basalts from the North Arch Volcanic Field, Hawaii: Extensive degassing of deep submarine-erupted alkali series lavas, *J. Petrol.*, *38*, 911–939, doi:10.1093/petroj/38.7.911.
Esposito, R., J. Hunter, J. D. Schiffbauer, N. Shimizu, and R. J. Bodnar (2014), An assessment of the reliability of melt inclusions as recorders of the pre-eruptive volatile content of magmas, *Am. Mineral.*, *99*, 976–998, doi:10.2138/am.2014.4574.
Gaetani, G. A., J. A. O'Leary, K. T. Koga, E. H. Hauri, E. F. Rose-Koga, and B. D. Monteleone (2014), Hydration of mantle olivine under variable water and oxygen fugacity conditions, *Contrib. Mineral. Petrol.*, *167*, 965–979, doi:10.1007/s00410-014-0965-y.
Galipp, K., A. Klügel, and T. H. Hansteen (2006), Changing depths of magma fractionation and stagnation during the evolution of an oceanic island volcano: La Palma (Canary Islands), *J. Volcanol. Geotherm. Res.*, *155*, 258–306, doi:10.1016/j.jvolgeores.2006.04.002.
Geldmacher, J., K. Hoernle, P. V. D. Bogaard, S. Duggen, and R. Werner (2005), New $^{40}Ar/^{39}Ar$ age and geochemical data from seamounts in the Canary and Madeira volcanic provinces: Support for the mantle plume hypothesis, *Earth Planet. Sci. Lett.*, *237*, 85–101, doi:10.1016/j.epsl.2005.04.037.
González, P. J., S. V. Samsonov, S. Pepe, K. F. Tiampo, P. Tizzani, F. Casu, J. Fernández, A. G. Camacho, and E. Sansosti (2013), Magma storage and migration associated with the 2011–2012 El Hierro eruption: Implications for crustal magmatic systems at oceanic island volcanoes, *J. Geophys. Res.*, *118*, 4361–4377, doi:10.1002/jgrb.50289.
Guillou, H., J. C. Carracedo, R. Paris, and F. J. Pérez Torrado (2004), K/Ar ages and magnetic stratigraphy of the Miocene–Pliocene shield volcanoes of Tenerife, Canary Islands: Implications for the early evolution of Tenerife and the Canarian hotspot age progression, *Earth Planet. Sci. Lett.*, *222*, 599–614.
Gurenko, A. A., and H.-U. Schmincke (2000), S concentrations and its speciation in Miocene basaltic magmas north and south of Gran Canaria (Canary Islands): Constraints from glass inclusions in olivine and clinopyroxene, *Geochim. Cosmochim. Acta*, *64*, 2321–2337.
Gurenko, A. A., T. H. Hansteen, and H. U. Schmincke (1996), Evolution of parental magmas of Miocene shield basalts of Gran Canaria (Canary Islands): Constraints from crystal, melt and fluid inclusions in minerals, *Contrib. Mineral. Petrol.*, *124*, 422–435.
Hamada, M., T. Kawamoto, E. Takahashi, and T. Fujii (2011), Polybaric degassing of island arc low-K tholeiitic basalt magma recorded by OH concentrations in Ca-rich plagioclase, *Earth Planet. Sci. Lett.*, *308*, 259–266.
Hammer, J. E., and M. J. Rutherford (2003), Petrologic indicators of pre-eruptions magma dynamics, *Geology*, *31*, 79–82, doi:10.1130/0091-7613(2003)031<0079:PIOPMD>2.0.CO;2.
Hansteen, T. H., and V. R. Troll (2003), Oxygen isotope composition of xenoliths from the oceanic crust and volcanic edifice beneath Gran Canaria (Canary Islands): Consequences for crustal contamination of ascending magmas, *Chem. Geol.*, *193*, 181–193, doi:10.1016/S0009-2541(02)00325-X.
Hansteen, T. H., A. Klügel, and H.-U. Schmincke (1998), Multi-stage magma ascent beneath the Canary Islands: Evidence from fluid inclusions, *Contrib. Mineral. Petrol.*, *132*, 48–64, doi:10.1007/s004100050404.
Hauri, E. H., G. A. Gaetani, and T. H. Green (2006), Partitioning of water during melting of the Earth's upper mantle at H_2O-undersaturated conditions, *Earth Planet. Sci. Lett.*, *248*, 715–734, doi:10.1016/j.epsl.2006.06.014.
Hauri, E. H., T. Weinreich, A. E. Saal, M. C. Rutherford, and J. A. Van Orman (2011), High pre-eruptive water contents preserved in lunar melt inclusions, *Science*, *333*, 213–215, doi:10.1126/science.1204626.
Hercule, S., and J. Ingrin (1999), Hydrogen in diopsides: Diffusion, kinetics of extraction-incorporation, and solubility, *Am. Mineral.*, *84*, 1577–1587.
Hoernle, K. (1998), Trace element and Sr-Nd-Pb isotopic geochemistry of Jurassic ocean crust beneath Gran Canaria (Canary Islands): Implications for the generation of OIB reservoirs and for crustal contamination of ascending OIB magmas, *J. Petrol.*, *39*, 859–880.
Hoernle, K., and H. U. Schmincke (1993a), The role of partial melting in the 15-Ma geochemical evolution of Gran Canaria: A blob model for the Canary hotspot, *J. Petrol.*, *34*, 599–626, doi:10.1093/petrology/34.3.599.
Hoernle, K., and H. U. Schmincke (1993b), The petrology of the tholeiites through melilite nephelinites on Gran Canaria, Canary Islands: Crystal fractionation, accumulation, and depths of melting, *J. Petrol.*, *34*, 573–597.

Hoernle, K., Y.-S. Zhang, and D. Graham (1995), Seismic and geochemical evidence for large scale mantle upwelling beneath the eastern Atlantic and western and central Europe, *Nature*, *374*, 34–39, doi:10.1038/374034a0.

Ingrin, J., and M. Blanchard (2006), Diffusion of hydrogen in minerals, *Rev. Mineral. Geochem.*, *62*, 291–320, doi:10.2138/rmg.2006.62.13.

Ingrin, J., and H. Skogby (2000), Hydrogen in nominally anhydrous upper-mantle minerals: Concentration levels and implications, *Eur. J. Mineral.*, *12*, 543–570.

Irvine, T. N., and W. R. A. Baragar (1971), A guide to the chemical classification of the common volcanic rocks, *Can. J. Earth Sci.*, *8*, 523–548, doi:10.1139/e71-055.

Klügel, A. (1998), Reactions between mantle xenoliths and host magma beneath La Palma (Canary Islands): Constraints on magma ascent rates and crustal reservoirs, *Contrib. Mineral. Petrol.*, *131*, 237–257, doi:10.1007/s004100050391.

Klügel, A., K. A. Hoernle, H.-U. Schmincke, and J. D. L. White (2000), The chemically zoned 1949 eruption on La Palma (Canary Islands): Petrologic evolution and magma supply dynamics of a rift zone eruption, *J. Geophys. Res.*, *105*, 5997–6016, doi:10.1029/1999JB900334.

Klügel, A., T. H. Hansteen, and K. Galipp (2005), Magma storage and underplating beneath Cumbre Vieja volcano, La Palma (Canary Islands), *Earth Planet. Sci. Lett.*, *236*, 211–226, doi:10.1016/j.epsl.2005.04.006.

Koch-Müller, M., I. Abs-Wurmbach, D. Rhede, V. Kahlenberg, and S. Matsyuk (2007), Dehydration experiments on natural omphacites: Qualitative and quantitative characterization by various spectroscopic methods, *Phys. Chem. Mineral.*, *34*, 663–678.

Kovalenko, V. I., V. B. Naumov, A. V. Girnis, V. A. Dorofeeva, and V. V. Yarmolyuk (2007), Volatiles in basaltic magmas of ocean islands and their mantle sources: I. Melt compositions deduced from melt inclusions and glasses in the rocks, *Geochem. Int.*, *45*, 313–326, doi:10.1134/S0016702907020012.

Lange, R. A., H. M. Frey, and J. Hector (2009), A thermodynamic model for the plagioclase-liquid hygrometer/thermometer, *Am. Mineral.*, *94*, 494–506.

LeBas, M. J., D. C. Rex, and C. J. Stillman (1986), The early magmatic chronology of Fuerteventura, Canary Islands, *Geol. Mag.*, *123*, 287–298.

Le Maitre, R. W., et al. (1989), *A Classification of Igneous Rocks and Glossary of Terms*, Blackwell, Oxford, U. K.

Le Voyer, M., P. D. Asimow, J. L. Mosenfelder, Y. Guan, P. J. Wallace, P. Schiano, E. M. Stolper and J. M. Eiler (2014), Zonation of H_2O and F concentrations around melt inclusions in olivines, *J. Petrol.*, *55*(4), 685–707, doi:10.1093/petrology/egu003.

Libowitzky, E., and G. R. Rossman (1997), An IR absorption calibration for water in minerals, *Am. Mineral.*, *82*, 1111–1115.

Longpré, M. A., V. R. Troll, and T. H. Hansteen (2008), Upper mantle magma storage and transport under a Canarian shield-volcano, Teno, Tenerife (Spain), *J. Geophys. Res.*, *113*, B08203, doi:10.1029/2007JB005422.

Longpré, M. A., V. R. Troll, T. R. Walter, and T. H. Hansteen (2009), Volcanic and geochemical evolution of the Teno massif, Tenerife, Canary Islands: Some repercussions on giant landslides on ocean island magmatism, *Geochem. Geophys. Geosyst.*, *10*, Q12017, doi:10.1029/2009GC002892.

Longpré, M. A., A. Klügel, A. Diehl, and J. Stix (2014), Mixing in mantle magma reservoirs prior to and during the 2011–2012 eruption at El Hierro, Canary Islands, *Geology*, *42*, 315–318, doi:10.1130/G35165.1.

Malfait, W. J., R. Seifert, S. Petitgirard, M. Mezouar, and C. Sanchez-Valle (2014), The density of andesitic melts and the compressibility of dissolved water in silicate melts at crustal and upper mantle conditions, *Earth Planet. Sci. Lett.*, *393*, 31–38, doi:10.1016/j.epsl.2014.02.042.

Manconi, A., M.-A. Longpré, T. R. Walter, V. R. Troll, and T. H. Hansteen (2009), The effects of flank collapses on volcano plumbing systems, *Geology*, *37*, 1099–1102, doi:10.1130/G30104A.1.

Martí, J., A. Castro, C. Rodríguez, F. Costa, S. Carrasquilla, R. Pedreira, and X. Bolos (2013a), Correlation of magma evolution and geophysical monitoring during the 2011–2012 El Hierro (Canary Islands) submarine eruption, *J. Petrol.*, *54*, 1349–1373, doi:10.1093/petrology/egt014.

Martí, J., V. Pinel, C. López, A. Geyer, R. Abella, M. Tárraga, M. José Blanco, A. Castro, and C. Rodríguez (2013b), Causes and mechanisms of the 2011–2012 El Hierro (Canary Islands) submarine eruption, *J. Geophys. Res. Solid Earth*, *118*, 823–839, doi:10.1002/jgrb.50087.

Massare, D., N. Métrich, and R. Clocchiatti (2002), High-temperature experiments on silicate melt inclusions in olivine at 1 atm: Inference on temperatures of homogenization and H_2O concentrations, *Chem. Geol.*, *183*, 87–98, doi:10.1016/S0009-2541(01)00373-4.

McDougall, I., and H. U. Schmincke (1976), Geochronology of Gran Canaria, Canary Islands: Age of shield building volcanism and other magmatic phases, *Bull. Volcanol.*, *40*, 1–21, doi:10.1007/BF02599829.

Mollo, S., P. Del Gaudio, G. Ventura, G. Iezzi, and P. Scarlato (2010), Dependence of clinopyroxene composition on cooling rate in basaltic magmas: Implications for thermobarometry, *Lithos*, *118*, 302–312, doi:10.1016/j.lithos.2010.05.006.

Montelli, R., G. Nolet, F. A. Dahlen, G. Masters, E. R. Engdahl, and S.-H. Hung (2004), Finite frequency tomography reveals a variety of plumes in the mantle, *Science*, *303*, 338–343, doi:10.1126/science.1092485.

Montelli, R., G. Nolet, F. A. Dahlen, and G. Masters (2006), A catalogue of deep mantle plumes: New results from finite-frequency tomography, *Geochem. Geophys. Geosyst.*, *7*, Q11007, doi:10.1029/2006GC001248.

Moore, J. G. (1970), Water content of basalt erupted on the ocean floor, *Contrib. Mineral. Petrol.*, *28*, 272–279, doi:10.1007/BF00388949.

Morimoto, N., J. Fabries, A. K. Ferguson, I. V. Ginzburg, M. Ross, F. A. Seifert, J. Zussman, K. Aoki, and G. Gottardi (1988), Nomenclature of pyroxenes, *Am. Mineral.*, *73*, 1123–1133, doi:10.1007/BF01226262.

Moune, S., O. Sigmarsson, T. Thordarson, and P.-J. Gauthier (2007), Recent volatile evolution in the magmatic system of Hekla volcano, Iceland, *Earth Planet. Sci. Lett.*, *255*, 373–389, doi:10.1016/j.epsl.2006.12.024.

Nazzareni, S., H. Skogby and P. F. Zanazzi (2011), Hydrogen content in clinopyroxene phenocrysts from Salina mafic lavas (Aeolian arc, Italy), *Contrib. Mineral. Petrol.*, *162*, 275–288, doi:10.1007/s00410-010-0594-z.

Nikogosian, I. K., T. Elliott, and J. L. R. Touret (2002), Melt evolution beneath thick lithosphere: A magmatic inclusion study of La Palma, Canary Islands, *Chem. Geol.*, *183*, 169–193.

Okumura, S. (2011), The H_2O content of andesitic magmas from three volcanoes in Japan, inferred from the infrared analysis of clinopyroxene, *Eur. J. Mineral.*, *23*, 771–778, doi:10.1127/0935-1221/2011/0023-2141.

O'Leary, J. A., G. A. Gaetani, and E. H. Hauri (2010), The effect of tetrahedral Al3+ on the partitioning of water between clinopyroxene and silicate melt, *Earth Planet. Sci. Lett.*, *297*, 111–120.

Plank, T., K. A. Kelley, M. M. Zimmer, E. H. Hauri, and P. J. Wallace (2013), Why do mafic arc magmas contain ~4 wt% water on average?, *Earth Planet. Sci. Lett.*, *364*, 168–179, doi:10.1016/j.epsl.2012.11.044.

Portnyagin, M., R. Almeev, S. Matveev, and F. Holtz (2008), Experimental evidence for rapid water exchange between melt inclusions in olivine and host magma, *Earth Planet. Sci. Lett.*, *272*, 541–552, doi:10.1016/j.epsl.2008.05.020.

Prescher, C., C. McCammon, and L. Dubrovinsky (2012), MossA: A program for analyzing energy-domain Mössbauer spectra from conventional and synchrotron sources, *J. Appl. Crystallogr.*, *45*, 329–331, doi:10.1107/S0021889812004979.

Putirka, K., M. Johnson, R. Kinzler and D. Walker (1996), Thermobarometry of mafic igneous rocks based on clinopyroxene-liquid equilibria, 0–30 kbar, *Contrib. Mineral. Petrol.*, *123*, 92–108, doi:10.1007/s004100050145.
Putirka, K. D. (2008), Thermometers and barometers for volcanic systems, *Rev. Mineral. Geochem.*, *69*, 61–120, doi:10.2138/rmg.2008.69.3.
Putirka, K. D. and C. Condit (2003), Cross section of a magma conduit system at the margins of the Colorado Plateau, *Geology*, *31*, 701–704, doi:10.1130/G19550.1.
Putirka, K. D., H. Mikaelian, F. Ryerson and H. Shaw (2003), New clinopyroxene–liquid thermobarometers for mafic, evolved, and volatile-bearing lava compositions, with applications to lavas from Tibet and the Snake River Plain, Idaho, *Am. Mineral.*, *88*, 1542–1554.
Rancourt, D. G., and J. Y. Ping (1991), Voigt-based methods for arbitrary-shaped static hyperfine parameter distributions in Mössbauer spectroscopy, *Nucl. Instrum. Methods Phys. Res., Sect. B*, *52*, 85–97, doi:10.1016/0168-583X(91)95681-3.
Roggensack, K., R. L. Hervig, S. B. McKnight, and S. N. Williams (1997), Explosive basaltic volcanism from Cerro Negro volcano: Influence of volatiles on eruptive style, *Science*, *277*, 1639–1642, doi:10.1126/science.277.5332.1639.
Rutherford, M. J., and J. D. Devine (1996), Pre-eruption pressure–temperature conditions and volatiles in the 1991 dacitic magma of Mount Pinatubo, in *Fire and Mud: Eruptions and Lahars of Mount Pinatubo, Philippines*, edited by C. G. Newhall and R. S. Punongbayan, pp. 751–766, Univ. of Wash. Press, Seattle, Wash.
Rutherford, M. J., H. Sigurdsson, S. Carey, and A. Davis (1985), The May 18, 1980, eruption of Mount St. Helens: Melt composition and experimental phase equilibria, *J. Geophys. Res.*, *90*, 2929–2947, doi:10.1029/JB090iB04p02929.
Schwarz, S., A. Klügel, and C. Wohlgemuth-Ueberwasser (2004), Melt extraction pathways and stagnation depths beneath the Madeira and Desertas rift zones (NE Atlantic) inferred from barometric studies, *Contrib. Mineral. Petrol.*, *147*, 228–240, doi:10.1007/s00410-004-0556-4.
Sides, I. R., M. Edmonds, J. Maclennan, D. A. Swanson, and B. F. Houghton (2014), Eruption style at Kilauea Volcano in Hawaii linked to primary melt composition, *Nat. Geosci.*, *7*, 464–469, doi:10.1038/ngeo2140.
Skogby, H. (1994), OH incorporation in synthetic clinopyroxenes, *Am. Mineral.*, *79*, 240–249.
Skogby, H. (2006), Water in natural mantle minerals I: Pyroxenes, *Rev. Mineral. Geochem.*, *62*, 155–168, doi:10.2138/rmg.2006.62.7.
Skogby, H. and G. R. Rossman (1989), OH- in pyroxene: An experimental study of incorporation mechanisms and stability, *Am. Mineral.*, *74*, 1059–1069.
Stalder, R. (2004), Influence of Fe, Cr and Al on hydrogen incorporation in orthopyroxene, *Eur. J. Mineral.*, *16*, 703–711.
Stalder, R., and T. Ludwig (2007), OH incorporation in synthetic diopside, *Eur. J. Mineral.*, *19*, 373–380.
Staudigel, H., and H.-U. Schmincke (1984), The Pliocene seamount series of La Palma/Canary Islands, *J. Geophys. Res.*, *89*, 11,195–11,215, doi:10.1029/JB089iB13p11195.
Stroncik, N. A., A. Klügel, and T. H. Hansteen (2009), The magmatic plumbing system beneath El Hierro (Canary Islands): Constraints from phenocrysts and naturally quenched basaltic glasses in submarine rocks, *Contrib. Mineral. Petrol.*, *157*, 593–607, doi:10.1007/s00410-008-0354-5.
Sundvall, R., and H. Skogby (2011), Hydrogen defect saturation in natural pyroxene, *Phys. Chem. Miner.*, *38*, 335–344, doi:10.1007/s00269-010-0407-y.
Sundvall, R., and R. Stalder (2011), Water in upper mantle pyroxene megacrysts and xenocrysts: A survey study, *Am. Mineral.*, *96*, 1215–1227.
Sundvall, R., H. Skogby and R. Stalder (2009), Dehydration-hydration mechanisms in synthetic Fe-poor diopside, *Eur. J. Mineral.*, *21*, 17–26, doi:10.1127/0935-1221/2009/0021-1880.
Tenzer, R., M. Bagherbandi, and P. Vajda (2013), Global model of the upper mantle lateral density structure based on combining seismic and isostatic models, *Geosci. J.*, *17*(1), 65–73, doi:10.1007/s12303-013-0009-z.
Thomas, R. (2000), Determination of water contents of granite melt inclusions by confocal laser Raman microprobe spectroscopy, *Am. Mineral.*, *85*, 868–872.
Vigouroux, N., P. J. Wallace, G. Williams-Jones, K. Kelley, A. J. R. Kent and A. E. Williams-Jones (2012), The sources of volatile and fluid-mobile elements in the Sunda arc: A melt inclusion study from Kawah Ijen and Tambora volcanoes, Indonesia, *Geochem. Geophys. Geosyst.*, *13*, Q09015, doi:10.1029/2012GC004192.
Wade, J. A., T. Plank, E. H. Hauri, K. A. Kelley, K. Roggensack, and M. Zimmer (2008), Prediction of magmatic water contents via measurement of H_2O in clinopyroxene phenocrysts, *Geology*, *36*, 799–802, doi:10.1130/G24964A.1.
Walker, J. A., K. Roggensack, L. C. Patino, B. I. Cameron, and O. Matías (2003), The water and trace element contents of melt inclusions across an active subduction zone, *Contrib. Mineral. Petrol.*, *146*, 62–77, doi:10.1007/s00410-003-0482-x.
Wallace, P. J. (1998), Pre-eruptive H_2O and CO_2 contents of mafic magmas from the submarine to emergent shield stages of Gran Canaria, in *Proceedings of the Ocean Drilling Program, Scientific Results*, edited by P. P. E. Weaver et al., vol. 157, pp. 411–420, Ocean Drill. Program, College Station, Tex.
Wallace, P. J. (2005), Volatiles in subduction zone magmas: Concentrations and fluxes based on melt inclusion and volcanic gas data, *J. Volcanol. Geotherm. Res.*, *140*, 217–240, doi:10.1016/j.jvolgeores.2004.07.023.
Walter, T. R., and V. R. Troll (2003), Experiments on rift zone formation in unstable volcanic edifices, *J. Volcanol. Geotherm. Res.*, *127*, 107–120, doi:10.1016/S0377-0273(03)00181-1.
Waters, L. E., and R. A. Lange (2015), An updated calibration of the plagioclase-liquid hygrometer-thermometer applicable to basalts through rhyolites, *Am. Mineral.*, in press, doi:10.2138/am-2015-5232.
Woods, A. W., and T. Koyaguchi (1993), Transitions between explosive and effusive eruptions of silicic magmas, *Nature*, *370*, 641–644, doi:10.1038/370641a.
Woods, S. C., S. Mackwell, and D. Dyar (2000), Hydrogen in diopside: Diffusion profiles, *Am. Mineral.*, *85*, 480–487.
Zaczek, K., V. R. Troll, M. Cachao, J. Ferreira, F. M. Deegan, J. C. Carracedo, V. Soler, F. C. Meade, and S. Burchardt (2015), Nannofossils in 2011 El Hierro eruptive products reinstate plume model for Canary Islands, *Sci. Rep.*, *5*, Article 7954, doi:10.1038/srep07945.